**Assessment of soil liquefaction potential using genetic programming using a probability-based approach.**

**Nerusupalli Dinesh Kumar Reddy* , Prof Ashok Kumar Gupta[2] , Prof Anil Kumar Sahu[3]**

**Department of Civil Engineering, Delhi Technological University, 110042, India.**

**Email: dkumarreddy_phd2k18@dtu.ac.in**

**Email: akgupta@dtu.ac.in**

**Email: Kumar.civil2018@gmail.com**

*Corresponding Author: (dkumarreddy_phd2k18@dtu.ac.in)

**Abstract**

Soil liquefaction is a substantial seismic hazard that endangers both human life and infrastructure. This research specifically examines the occurrence of soil liquefaction events in past earthquakes, with a special emphasis on the 1964 Niigata, Japan and 1964 Alaska, USA earthquakes. These occurrences were important achievements in the comprehension of harm caused by liquefaction. Geotechnical engineers often use in-situ experiments, such as the standard penetration test (SPT) to evaluate the likelihood of liquefaction. The attraction for this option arises from the difficulties connected in acquiring undisturbed samples of superior quality, as well as the related expenses. Geotechnical engineering specialists choose the deterministic framework for liquefaction assessment because of its clear mathematical approach and low needs for data, time, and effort. This work emphasises the need of integrating probabilistic and reliability methodologies into the design process of crucial life line structures to enable well-informed risk-based decision-making. The objective of this project is to create models that use deterministic, probabilistic, and reliability-based methods to evaluate the likelihood of soil liquefaction. The work presents a new equation that combines Bayes conditional probability with Genetic Programming (GP). and also in study is to identify the most suitable method for liquefaction analysis based on factor of safety and Performance Fitness Error Metrics (PFEMs), Rank analysis, Gini index, etc. The information provided in study data include soil and seismic characteristics, including the corrected blow count $(N1)60cs$, fines content (FC), mean grain size ($D50$), peak horizontal ground surface acceleration ($amax$), earthquake magnitude (M), and $CSR7.5$. The parameters are derived from the SPT measurements conducted at many global locations, together with field performance observations (LI) and probability of liquefaction has been assessed through the use of Gini Index (GI). A comparison was made between the novel methodology and the techniques proposed by Juang et al. (2002), Toprak et al. (1999), and Idriss and Boulanger (2006) status of case history data using Performance Fitness Error Metrices. The comparison included employing a confusion matrix for binary classification and doing a score analysis based on factor ranking. The proposed model exhibited superior performance, as the outputs of the constructed model increased for all positive factors and decreased for negative indicators.

## 1. Introduction

Seismic hazards include many threats such as ground shaking, structural vulnerabilities, liquefaction, landslides, failures of retaining structures, dangers to essential infrastructure, and tsunamis. The primary cause of both human casualties and infrastructure damage is the liquefaction of soil triggered by seismic activity. Terzhagi and Peck (1948) were the first to recognise and describe the occurrence of soil liquefaction, which refers to the abrupt decrease in strength of loose sand deposits. This discovery played a crucial role in the early development of soil mechanics. The key factor leading to slope collapse in saturated sand deposits was identified. However, it was the occurrence of severe earthquakes in various parts of the world, such as Niigata and Alaska (1964), Loma Prieta (1989), Kobe (1995), Kocaeli (1999), and Chi-Chi (1999), that drew the attention of engineers, seismologists, and the scientific community to this phenomenon (Baziar and Jafarian, 2007). Subsequent research conducted in both field and laboratory settings has demonstrated that soil liquefaction can be better characterised as a disastrous failure event. This occurs when saturated soil experiences a loss of strength caused by a rise in pore water pressure and a decrease in effective stress due to rapid loading. As a result, the soil becomes mobile enough to move over distances ranging from metres to kilometres. Soil liquefaction may cause ground failure, such as the emergence of sand boils, large landslides, surface sinking, lateral spreading, movement of bridge supports, settling and swaying of buildings, collapse of marine structures, and extensive damage to lifeline systems, among other consequences.

The simplified approach based on the Standard Penetration Test (SPT), first devised by Seed and Idriss in 1971, At the same time, Tsuchida and Hayashi (1971) developed a relation between the grain-size distribution and liquefaction susceptibility of soils using the Japanese liquefaction sites. In the later stage, based on this “simplified procedure” researchers have attempted to build more accurate deterministic and probabilistic triggering correlations using the SPT data (Seed and Idriss 1982; Seed et al. 1983; Seed et al. 1985; Youd et al. 2001), It remains the most often used method globally. Robertson and Campanella (1985) pioneered the development of a CPT-based technique for assessing the likelihood of liquefaction, this method involves converting the SPT-based approach by using an empirical correlation between SPT-CPT, it follows a stress-based approach similar to the one proposed by Seed and Idriss (1971). Further Several improvements done for on cone penetration testing (CPT) by using statistical and regression analysis techniques methods (Seed and de Alba (1986), Olsen (1988), Shibata and Teparaksa (1988), Mitchell and Tseng (1990), Stark and Olson (1995), Suzuki et al. (1995), Olsen (1997), Robertson and Wride (1998), and Youd et al. (2001).) Multiple simpler procedures using shear wave velocity VS have been developed (Stokoe et al. 1988; Tokimatsu and Uchida 1990; Addo and Robertson 1992; Kayen et al. 1992; Andrus and Stokoe 2000; Juang et al. 2000; Juang et al. 2001; Andrus et al. 2004). There are only a limited number of simpler techniques based on the BPT (Becker Penetration Test) technique which was proposed by Harder and Seed (1986). These methods, however, are only applicable to soils with a gravelly composition.

The boundary curve provides the liquefaction resistance of a soil, usually stated as the cyclic resistance ratio (CRR), for a certain index of soil resistance, such as the corrected SPT impact count. The evaluation of a soil's liquefaction potential under seismic loading involves assessing the factor of safety ($Fs$), which is determined by the ratio of the cyclic resistance ratio (CRR) to the cyclic stress ratio (CSR). The seismic loading is commonly

stated as CSR. The deterministic technique, which involves quantifying the liquefaction potential of soil in terms of the factor of safety ($Fs$), is preferred by geotechnical specialists for its simplicity in implementation. Parametric and model inaccuracies may lead to situations where $Fs$>1 does not always indicate the absence of soil liquefaction, nor does it guarantee a complete absence of the risk of liquefaction. Furthermore, it should be noted that $Fs$ does not always result in liquefaction and does not guarantee complete liquefaction, as stated by Juang et al. (2000). In deterministic methodologies, the interface between liquefaction and non-liquefaction scenarios is known as a performance function or "limit state function." This function is often designed to be conservative, including the majority of liquefied instances.

In recent decades, some geotechnical researchers have successfully forecasted the probability of liquefaction by using reliability analysis, taking into consideration mistakes in models and parameters (Haldar and Tang 1979; Liao et al. 1988; Toprak et al. 1999; Juang et al. 2006; Idriss and Boulanger 2006.) performed a logistic regression analysis on the available case histories in order to ascertain the probability of liquefaction ($P_L$). These studies propose a simple regression equation that may be used to estimate the nominal probability, which is a measure of the model's level of uncertainty.

Juang et al. (1999) developed a dependable technique for estimating the likelihood of liquefaction ($P_L$) using a Bayesian mapping function. Juang et al. (2002) further developed their previously suggested approach for creating a mapping function that relates $P_L$ and $Fs$. This mapping function was constructed using the methodology proposed by Youd and Idriss (2001). Goharzay et al. (2017) built upon the first proposal of the first order reliability-based Bayes probability function by Muduli and Das (2015). The Bayesian network (BN) approach has been shown to be a very effective method for engineers to assess the probability of earthquake-induced liquefaction. Hu (2021a) introduced an innovative approach for forecasting the liquefaction of soil containing gravel this technique relies on the use of two Bayesian network models. Hu et al. (2022) developed a hybrid Bayesian network (BN) model to predict liquefaction caused by earthquakes. The model is based on shear wave velocity ($Vs$) and builds upon previous studies by Hu and Liu (2019); Hu (2021b); Hu et al. (2022); Pirhadi et al. (2023). In their study, used Cetin et al. (2004) database of case histories to establish a new collection of probabilistic and deterministic connections. Their objective was to predict the likelihood of liquefaction start by using the maximum likelihood function inside a Bayesian framework. Subsequently, Idriss and Boulanger (2010) and Boulanger and Idriss (2014) devised a method that combines deterministic and probabilistic approaches using SPT data, therefore enhancing the methodology established by Seed and Idriss (1971). The determination of liquefaction potential relies on a set of assumptions and approximations, which form the basis of all suggested conventional techniques and empirical linkages.

Fundamentally, difficulties related to assessing liquefaction are very nonlinear. Some of geotechnical researchers developed machine learning methods to overcome the challenges posed by nonlinearity and other complexities in forecasting the likelihood of liquefaction. Goh (1994) developed a neural network model to predict and evaluate the likelihood of liquefaction in saturated, cohesionless soil. The Artificial Neural Network (ANN) model, which is widely recognised as a leading machine learning approach in this field, has shown good use in the prediction of liquefaction (Samui and Sitharam 2011; Ramakrishnan et al. 2008). Subsequently, additional scholars in the geotechnical domain developed various machine learning techniques, such as neural networks, support vector machine (SVM), genetic programming (GP), least square support vector machine (LSSVM), and stochastic

gradient boosting (SGB), for the purpose of conducting liquefaction analysis (Pal 2006; Samui and Karthikeyan 2013; Hanna et al. 2007; Samui et al. 2011; Samui and Hariharan 2015; Xue and Liu 2017). Zhang et al. (2016) devised a non-parametric, multivariate adaptive regression spline (MARS) method to assess the likelihood of liquefaction in sands and granular soils using the energy concept. Zhang et al. (2021a) used CPT data to introduce the extreme learning machine (ELM) as a method for assessing the susceptibility of soil deposits to liquefaction. These basic models have some significant limitations, such as limited generalisation capacity, slow convergence rate, and susceptibility to overfitting. These shortcomings may adversely affect the accuracy of result prediction. The existing liquefaction assessment methods based on machine learning are fundamentally opaque since they favour accuracy at the expense of explainability. The existing liquefaction datasets are quite small and have a higher percentage of liquefaction events compared to non-liquefaction events. As a result, these models exhibit distinct performance characteristics when compared to databases from other areas of the world. Subsequently, additional scholars have introduced novel machine learning techniques such as random forest (RF) (Kohestani et al 2015), Jas and Dodagoudar (2023) proposed an explainable machine learning model for liquefaction potential assessment of soils using XGBoost-SHAP to address the issue of interpretability in the machine learning model, and gradient boosting machine (GBM) shown better adoptability to the low amount of data (Kumar et al. 2022a; Zou et al. 2019). Zhang and Wang (2021) have devised an improved ensembled and hybrid method using genetic algorithms and GWO, while Zhang et al. (2021b) have developed a hybrid model by incorporating SVM-GWO. Machine learning (ML) models that already exist are better options for handling enormous amounts of data and enhancing the accuracy of predictions. Every machine learning approach has its own limitations and constraints due to parameters and model ambiguity (Momeni et al., 2015).

## 2. Methodology

### 2.1 Introduction of prediction model and data base

A stress-based technique to evaluate the likelihood for liquefaction triggering was first devised by Seed and Idriss (1967). This methodology has been employed extensively over the course of the previous 45 years (Seed and Idriss 1971; Tokimatsu and Yoshimi 1983; *NRC* 1985; Seed et al. 1985; Youd et al. 2001; Cetin et al. 2004; Idriss and Boulanger 2004, 2008). The correlation between the cyclic resistance ratio (CRR) adjusted to a magnitude of 7.5 (M = 7.5) and the effective vertical stress ($\sigma_v' = 1$) and the corresponding value of the normalised cone penetration resistance $(N_1)_{60CS}$ for cohesionless soils, as determined by Idriss and Boulanger (2004, 2008), can be expressed as:

$$CSR_{7.5} = 0.65\frac{\sigma_v}{\sigma_y'}\frac{a_{max}}{g}r_d/MSFK_\sigma K_\propto \qquad (1)$$

$$CRR_{M=7.5,\sigma_v'=1atm} = exp\left(\left(\frac{(N_1)_{60cs}}{14.1}\right) + \left(\frac{(N_1)_{60cs}}{126}\right)^2 - \left(\frac{(N_1)_{60cs}}{23.6}\right)^3 + \left(\frac{(N_1)_{60cs}}{25.4}\right)^4 - 2.8\right) \qquad (2)$$

Where:

$amax$= surface peak acceleration

$\sigma v$= total overburden pressure

$\sigma' y$= effective overburden pressure

$rd$= reduction in shear stress in depth z

$K\sigma$ , $Ka$= correction factors

$MSF$= magnitude scaling factor

$(N1)60CS$= corrected SPT no

### 2.1.1 Deterministic methods ($F_S$)

In the approach, the $F_S$ parameter, which signifies the ratio of $CRR$ to $CSR$, is determined by forecasting individual values of load ($CSR$) and resistance ($CRR$) without considering the uncertainty related to the prediction of loading and resistance. Figure 2.8 illustrates this. The computed CRR and CSR are considered to have a probability of occurrence of 100%. Within a deterministic approach, a factor of safety ($F_S$) beyond 1 signifies the absence of liquefaction, whereas a $F_S$ value of 1 or below indicates the occurrence of liquefaction. The "simplified procedure" first introduced by Seed and Idriss (1971), and further explained in preceding sections, is the most definitive method for assessing the likelihood of liquefaction at a given site. This technique has been modified and improved several times to make it suitable for different in-situ testing scenarios (Seed et al., 1983; Seed et al., 1985; Robertson and Campanella, 1985; Shibata and Teparaksa, 1988; Olsen, 1997; Robertson and Wride, 1998). The 1998 workshop conducted by the National Centre for Earthquake Engineering Research ($NCEER$) resulted in a comprehensive assessment of deterministic methods that use in-situ testing to evaluate the potential occurrence of soil liquefaction (Youd et al., 2001). The equation may be used to compute the factor of safety ($Fs$) against liquefaction during an earthquake.

$$F_S = \left(\frac{CRR_{M=7.5,\sigma'_v=1atm} K_\sigma K_\alpha}{\text{CSR}*\text{MSF}}\right) \quad (3)$$

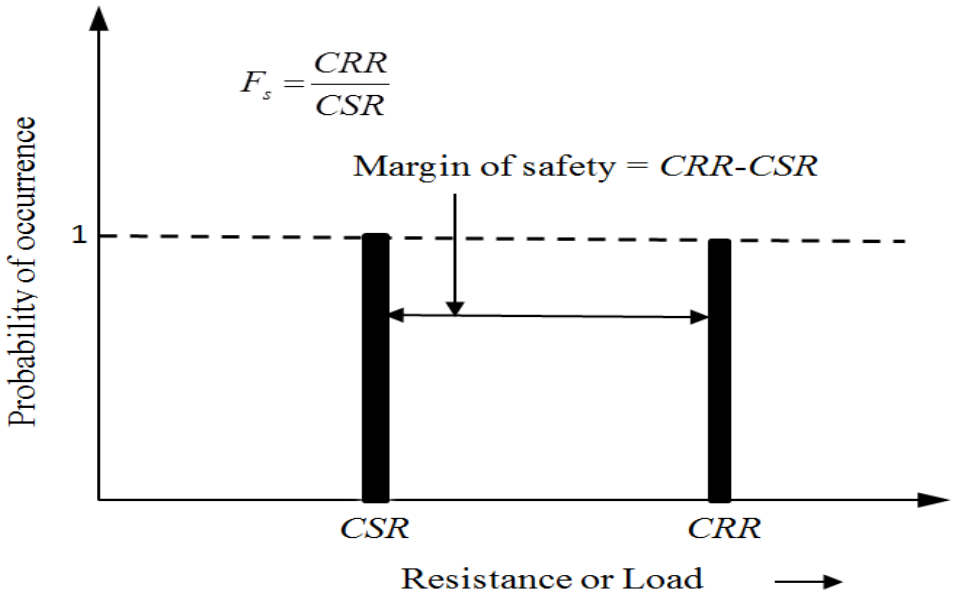

Figure 1. illustrates the deterministic technique used to evaluate liquefaction potential, as described by Becker (1997)

### 2.1.2 Data collection and processing

The current analysis used a dataset of measures acquired from the Standard Penetration Test (SPT). The collection included post-liquefaction case studies spanning from the Tohnankai earthquake in 1944 to the Chi Chi earthquake in 1999 in Taiwan. The dataset for the study included 286 instances of liquefaction and 210 instances of non-liquefaction. In addition, to verify the accuracy of the models, a set of 30 Standard Penetration Test (SPT) borehole data collected from Faridabad a region in the National Capital District (NCR) of Delhi. In the Figure .2 shown collection of sample setup and split spoon sampler. The bore hole data and the model data for the study are shown in Table 1 and Table 2, respectively.

Figure 2. (a) SPT field set up and (b) split spoon sample

Table 1 Sample bore hole data

| Avg Depth | WT | $\sigma_v$ (kPa) | $\sigma'_v$ (kPa) | $N_m$ | $(N_1)_{60}$ | $C_B$ | $C_E$ | $C_N$ | $C_R$ | $C_S$ | FC | $(N_1)_{60c}$ | $\Delta(N_1)_{60cs}$ | $\gamma_{total}$ | $\gamma'_{total}$ |
|---|---|---|---|---|---|---|---|---|---|---|---|---|---|---|---|

| | | | | | | | | | | | | | | | |
|---|---|---|---|---|---|---|---|---|---|---|---|---|---|---|---|
| 2.3 | 1.2 | 43 | 32 | 4 | 6.1 | 1 | 1.13 | 1.70 | 0.8 | 1 | 69 | 11.7 | 5 | 18.5 | 19.1 |
| 3.0 | 1.2 | 57 | 39 | 6 | 9.2 | 1 | 1.13 | 1.59 | 0.85 | 1 | 33 | 14.6 | 2 | 18.5 | 19.1 |
| 3.4 | 1.2 | 63 | 42 | 3 | 4.6 | 1 | 1.13 | 1.60 | 0.85 | 1 | 33 | 10.1 | 1 | 18.5 | 19.1 |
| 3.7 | 1.2 | 69 | 45 | 6 | 8.6 | 1 | 1.13 | 1.49 | 0.85 | 1 | 33 | 14.1 | 2 | 18.5 | 19.1 |
| 3.8 | 1.2 | 72 | 46 | 13 | 17.4 | 1 | 1.13 | 1.39 | 0.85 | 1 | 20 | 21.9 | 5 | 18.5 | 19.1 |
| 4.3 | 1.2 | 81 | 51 | 11 | 14.4 | 1 | 1.13 | 1.37 | 0.85 | 1 | 20 | 18.9 | 2 | 18.5 | 19.1 |
| 4.6 | 1.2 | 87 | 54 | 10 | 14.3 | 1 | 1.13 | 1.33 | 0.95 | 1 | 20 | 18.8 | 5 | 18.5 | 19.1 |
| 4.9 | 1.2 | 92 | 56 | 4 | 5.8 | 1 | 1.13 | 1.36 | 0.95 | 1 | 33 | 11.3 | 2 | 18.5 | 19.1 |
| 5.2 | 1.2 | 98 | 59 | 4 | 5.7 | 1 | 1.13 | 1.33 | 0.95 | 1 | 33 | 11.2 | 1 | 18.5 | 19.1 |
| 5.3 | 1.2 | 101 | 61 | 6 | 8.3 | 1 | 1.13 | 1.29 | 0.95 | 1 | 33 | 13.8 | 5 | 18.5 | 19.1 |
| 5.5 | 1.2 | 104 | 62 | 10 | 13.4 | 1 | 1.13 | 1.25 | 0.95 | 1 | 33 | 18.9 | 2 | 18.5 | 19.1 |
| 6.1 | 1.2 | 116 | 68 | 9 | 11.7 | 1 | 1.13 | 1.21 | 0.95 | 1 | 33 | 17.1 | 1 | 18.5 | 19.1 |
| 7.1 | 1.2 | 133 | 76 | 14 | 16.9 | 1 | 1.13 | 1.13 | 0.95 | 1 | 33 | 22.4 | 2 | 18.5 | 19.1 |
| 7.6 | 1.2 | 87 | 54 | 7.1 | 10.3 | 1 | 1.13 | 1.36 | 0.95 | 1 | 30 | 15.7 | 5.4 | 18.5 | 19.1 |

Table 2. sample trained and test data

| Liquefaction | Magnitude (M) | Critical Depth (d) | Fine Content (%) | D50 (mm) | Water Table (m) | PGA (g) | $r_d$ | (N1)60cs | CSR |
|---|---|---|---|---|---|---|---|---|---|
| Yes | 7.300 | 6.000 | 61.000 | 0.075 | 2.300 | 0.428 | 0.942 | 8.470 | 0.451 |
| Yes | 7.300 | 4.200 | 24.000 | 0.200 | 2.700 | 0.789 | 0.959 | 3.580 | 0.378 |
| Yes | 7.300 | 9.000 | 42.000 | 0.100 | 2.300 | 0.789 | 0.886 | 6.380 | 0.714 |
| Yes | 7.300 | 2.400 | 41.000 | 0.095 | 2.300 | 0.789 | 0.972 | 8.710 | 0.514 |
| Yes | 7.300 | 5.000 | 22.000 | 0.065 | 2.200 | 0.428 | 0.952 | 3.670 | 0.379 |

| | | | | | | | | | |
|---|---|---|---|---|---|---|---|---|---|
| Yes | 7.300 | 4.200 | 62.000 | 0.100 | 1.800 | 0.211 | 0.959 | 4.050 | 0.417 |
| Yes | 7.300 | 7.700 | 16.000 | 0.220 | 3.800 | 0.165 | 0.915 | 10.190 | 0.132 |
| Yes | 7.300 | 8.100 | 16.000 | 0.190 | 3.100 | 0.165 | 0.907 | 8.480 | 0.136 |
| Yes | 7.300 | 5.700 | 16.000 | 0.170 | 2.800 | 0.165 | 0.945 | 8.820 | 0.139 |
| Yes | 7.300 | 8.100 | 19.000 | 0.170 | 2.800 | 0.165 | 0.907 | 10.710 | 0.148 |
| Yes | 7.300 | 3.700 | 11.000 | 0.190 | 2.300 | 0.165 | 0.962 | 11.570 | 0.128 |
| Yes | 7.300 | 10.000 | 45.000 | 0.080 | 3.000 | 0.165 | 0.850 | 7.250 | 0.145 |
| Yes | 7.300 | 7.700 | 18.000 | 0.170 | 3.000 | 0.165 | 0.915 | 6.720 | 0.142 |
| No | 7.300 | 5.000 | 14.000 | 0.200 | 0.600 | 0.124 | 0.952 | 23.860 | 0.137 |
| No | 7.300 | 10.000 | 15.000 | 0.220 | 0.600 | 0.124 | 0.850 | 21.980 | 0.128 |
| No | 7.300 | 9.000 | 12.000 | 0.200 | 0.600 | 0.124 | 0.886 | 21.090 | 0.133 |
| No | 7.300 | 5.000 | 14.000 | 0.200 | 0.600 | 0.124 | 0.952 | 18.680 | 0.138 |
| No | 7.300 | 6.000 | 19.000 | 0.190 | 0.600 | 0.124 | 0.942 | 21.970 | 0.138 |
| No | 7.300 | 10.000 | 16.000 | 0.170 | 1.300 | 0.124 | 0.850 | 20.420 | 0.122 |
| No | 7.300 | 18.000 | 22.000 | 0.104 | 2.700 | 0.165 | 0.730 | 9.340 | 0.142 |
| No | 7.300 | 6.000 | 8.000 | 0.200 | 2.700 | 0.165 | 0.942 | 12.070 | 0.142 |
| No | 7.300 | 16.000 | 18.000 | 0.140 | 2.700 | 0.165 | 0.760 | 12.080 | 0.145 |
| No | 7.300 | 18.000 | 32.000 | 0.100 | 2.700 | 0.165 | 0.730 | 10.770 | 0.142 |
| No | 7.300 | 16.000 | 18.000 | 0.140 | 2.700 | 0.165 | 0.760 | 9.060 | 0.145 |
| No | 7.300 | 4.000 | 43.000 | 0.090 | 2.700 | 0.165 | 0.960 | 7.460 | 0.124 |
| No | 7.300 | 12.000 | 8.000 | 0.201 | 2.700 | 0.165 | 0.820 | 10.200 | 0.149 |

The sample bore hole data depth spans from 2.3 to 7.3 and has a water table depth of 1.2 metre, and SPT has been done and registered SPT no at different depths, and all adjustments are computed according to standard protocols supplied by previous studies. After calculating all variables, the corrected blow count $(N1)60cs$, fines content (FC), mean grain size ($D50$), peak horizontal ground surface acceleration (amax), magnitude of earthquake (M), shear stress reduction factor ($rd$), water table depth (WT), critical depth (d), and $CSR7.5$ were selected for further investigation.

The information provided in study data include soil and seismic characteristics, including the corrected blow count $(N1)60cs$, fines content (FC), mean grain size ($D50$), peak horizontal ground surface acceleration ($amax$), earthquake magnitude (M), and $CSR7.5$. The parameters are derived from the SPT measurements conducted at many global locations, together with field performance observations (LI). The soil in these circumstances may include sand, silty sand, sandy silt, and clayey silt. In terms of the database, the documented depths of SPT measurements range from 1.3 metres to 20.3 metres. The water table depth ranges from 0 to 15.30 metres. The range of values among $(N1)60cs$, is 0.93 to 35.22. The fines content (FC) number range from 0 to 92%. Conversely, the PGA value ranges from 0.052 to 1, while the $CSR7.5$ value ranges from 0.041 to 0.822. Based on the data, a total of 347 instances are randomly selected for training, while the remaining 149 cases are allocated for testing the developed model.

### 2.1.3 Data cleaning, normalization

Prior to constructing the model, it is necessary to preprocess the data in order to guarantee the precision of the model's predictions. The dataset has a minimal number of null values this time, and the conventional approach to address missing data is by using the empty value filling technique. To optimize the use of existing data and maintain the quantity and quality of samples, the 496 datasets may be enhanced by replacing the missing characteristic values with null values. By using statistical measures such as the average, median, quantile, complex, and random values of the whole dataset, one may assess the impact of various filling strategies. Ultimately, this article employs the most precise form of filling, which is the mean filling. All 10 parameters in the soil liquefaction dataset are numerical and exhibit varying ranges of values, which may fluctuate significantly in magnitude. The variability of values in the dataset might impact the rate at which the model converges. The features undergo min-max normalization to get precise classification outcomes and guarantee that each feature contributes significantly. Hence, data normalization guarantees that features with varying dimensions possess equal significance, hence enhancing the accuracy, speed of convergence, and stability of the model. Consequently, this leads to an improvement in the performance of machine learning algorithms. Every characteristic of the whole dataset is transformed to a range of values between 0 and 1 in order to minimize the influence of feature size and magnitude on the model. The min-max normalizing approach reduces the values of the features in a linear manner, while preserving the linear properties of the original dataset. The equation is as stated.

$$X' = \frac{X - Min(X)}{Max(X) - Min(X)} \tag{4}$$

### 2.1.4 Data Visualization and correlation analysis

The use of data visualization facilitates the comprehension of data trends, the interrelationships and distinctions among several variables employed in the study, and the level of disorder or randomness within the data. This understanding aids in determining appropriate methodologies for data analysis.

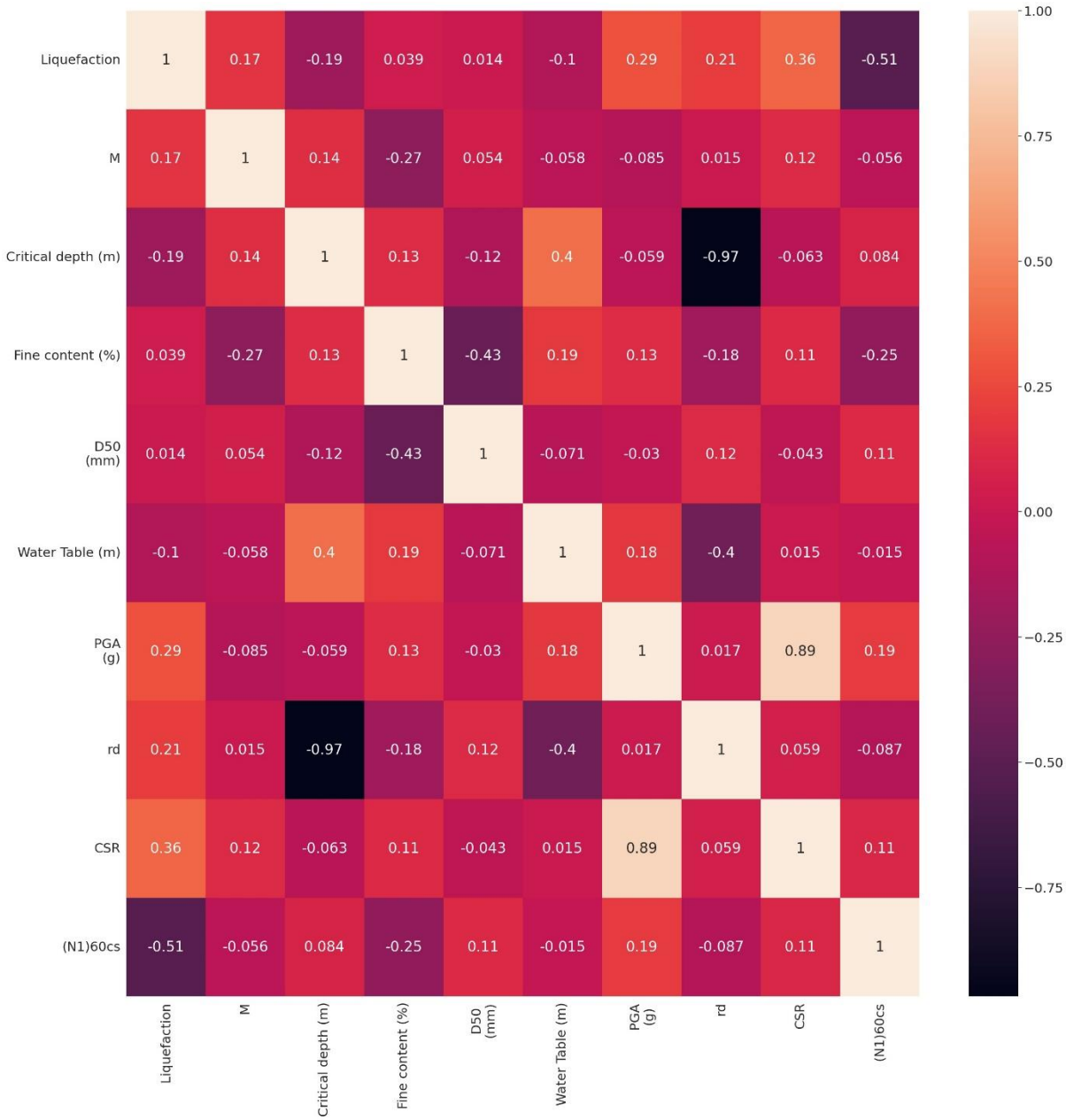


Figure 3. heat map of the Spearman's rank correlation coefficient matrix

A heat map of the Spearman's rank correlation coefficient matrix for the input variables is shown in Figure 3, with the corresponding correlation coefficients and diagonal element shown the target variable. It can be seen that parameters (Generally speaking, |R|= 0 implies an uncorrelated relationship; |R|< 0.2 implies a very weak correlation; 0.2 <|R|< 0.4 stands for a weak correlation; 0.4 <|R|< 0.6 stands for a moderate correlation; 0.6 <|R|<0.8 implies a strong correlation; 0.8 <|R|<1 implies a very strong correlation; |R|= 1 implies fully correlated.)

The formula for spearman's rank correlation coefficient is follows:

$$R = \frac{COV(rank\,(X) rank\,(Y))}{\sigma_{rank\,(X)}\sigma_{rank\,(Y)}} = \frac{\Sigma_i (R_X\,(i) - \overline{R_X})(R_Y\,(i) - \overline{R_Y})}{\sqrt{\Sigma_i (R_X\,(i) - \overline{R_X})^2}\sqrt{\Sigma_i (R_Y\,(i) - \overline{R_Y})^2}} \quad (5)$$

Where: $rank\,(X) rank\,(Y)$ are the ranks of variables $X, Y$, respectively $COV$ denotes covariance and $\sigma_{rank\,(X)} \sigma_{rank\,(Y)}$ are the standard deviations of $rank\,(X) rank\,(Y)$, $R_X, R_Y$ represents the average ranks for $rank\,(X) rank\,(Y)$, respectively.

Multicollinearity arises when predictor variables exhibit either positive or negative correlation. Positive correlation, as observed between variables X and Y, implies that they move in the same direction; when X increases, Y tends to increase. In regression, this strong positive relationship can lead to multicollinearity, hindering the model's ability to distinguish individual effects. Similarly, negative correlation, such as between variables A and B, involves opposite movements; as A increases, B tends to decrease. High negative correlations in regression may also result in multicollinearity issues, making it challenging to differentiate the impact of A and B on the outcome variable and potentially leading to unreliable estimates.

The variables Cyclic Stress Ratio (CSR) and Peak Ground Acceleration (PGA) exhibit a substantial positive correlation with a value of 0.89. This high correlation raises concerns about multicollinearity, suggesting the need to eliminate one of the variables. However, both variables are indispensable in liquefaction studies, necessitating their retention despite the correlation issue. Similarly, the Reduction Factor (rd) and Critical Depth (d) display a notable negative correlation of -0.97, which may also indicate multicollinearity. Despite this challenge, both variables remain crucial in liquefaction studies, and therefore, the decision is to retain both variables while acknowledging the potential impact of their high correlation.

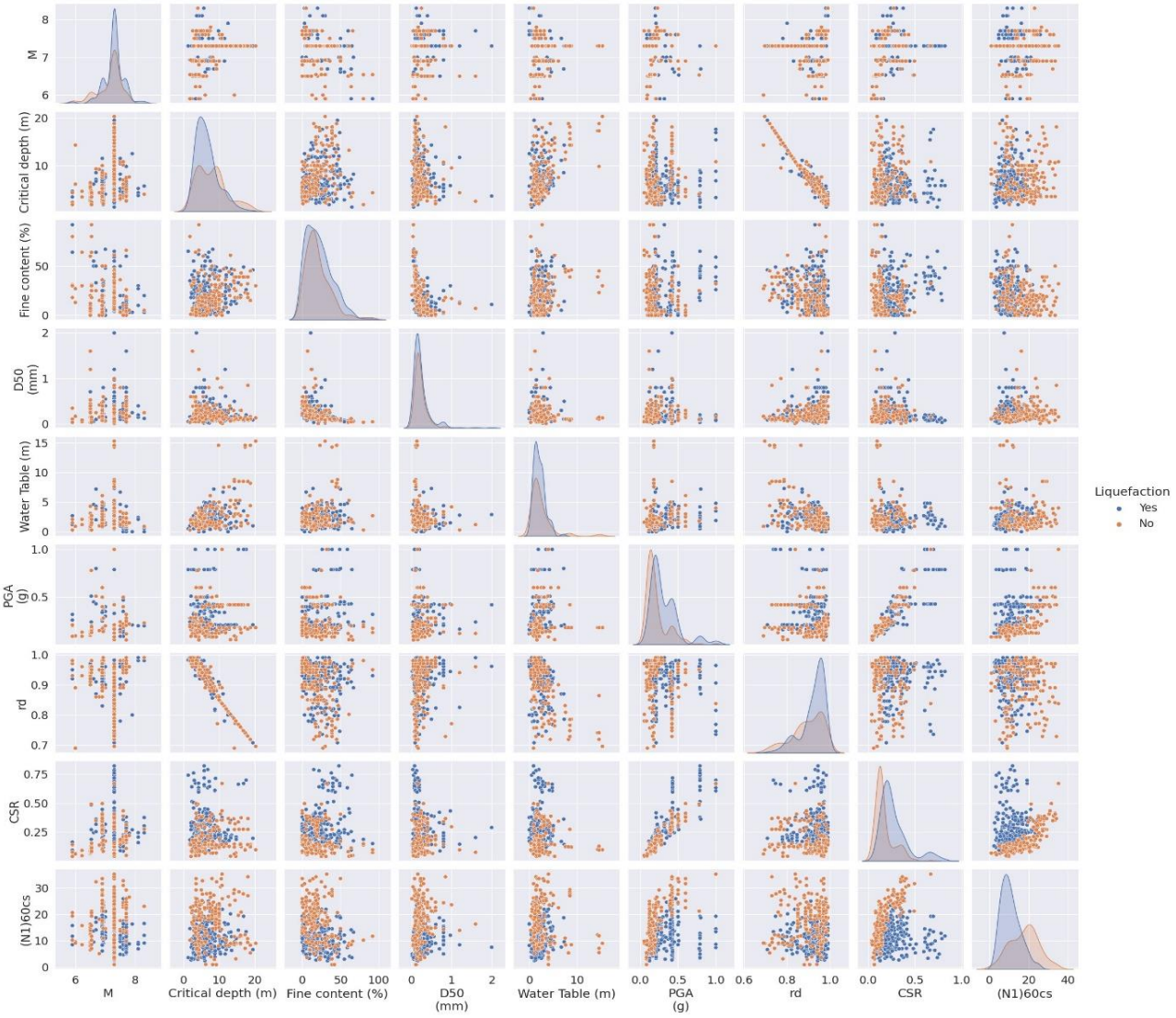


Figure 4. Pair plot to determine entropy of variables

Pair plot graphs are often used to assess the entropy of data, a lower entropy number indicates a substantial level of segregation or classification within the data, but a lower entropy value signifies a higher degree of information transmission. This entropy metric may provide a deeper comprehension of the selection of models, considering their categorization complexity and information transmission capabilities**.** Figure 4 depicts the contrast between data that has been liquefied and data that has non-liquefied, with respect to changes in the values of two variables. The Figure 4 clearly shows that there is no clear differentiation between the two types of data, suggesting a high level of complexity. Therefore, basic models are inadequate for analysing such intricate data. When faced with such a high degree of complexity, it is advisable to use more advanced models, such as genetic programming and advanced deep learning models, to get beneficial results.

**2.2 GEP model**

The computational approach known as GEP is applied to generate computer programs that contain the capacity to tackle difficult issues. Dr. Candida Ferreira first proposed the idea in 1992 as part of her PhD research at the University of Coimbra in Portugal. The GEP technique is based on the basic principles of genetics and natural

selection. The operating method of this system comprises the repeated development of a set of computer programs via a sequence of mutation and selection procedures. The GEP technique entails representing each program as a sequence of symbols that may undergo different genetic processes, such as combination and modification. By selecting programs with higher performance on a specific challenge in each generation and propagating them to the next generation, their overall fitness is improved over time. The capacity of GEP to manage numerous objectives concurrently renders it a valuable tool in the domain of optimization. The GEP has been extensively utilized in various domains, encompassing but not limited to data analysis, classification, and modelling. Empirical evidence suggests that GEP exhibits superior performance compared to other evolutionary computation techniques, including genetic programming and evolutionary strategies, in specific problem domains (Ferreira 2002). In addition, the GEP methodology has been expanded to accommodate intricate data structures, including trees and graphs, by implementing altered genetic operators (Oliveira et al. 2016).

The present investigation employs a modelling method that represents the objective value as CRR, while considering the five independent components as input variables. The model's structure was developed using GeneXproTools 5.0 (2023) in conjunction with the four fundamental arithmetic operators (+, −, ×, and /). The modelling process used high-quality datasets that were randomly distributed throughout two distinct periods. Table 3 displays many distinct models that were created for the present study. These models were generated by using varying ratios of training and testing datasets, employing diverse programme dimensions, and employing distinct generations. The root-mean-squared error (RMSE), denoted as Ei, was used as the fitness function in this specific experiment. The fitness (fi) was calculated by using an equation derived from the expression tree. This equation accounted for the overall number of errors relative to the desired value. The method of addition was used to form a link between the genetic components. The expression tree (ET) for the CRR of the GP model 3 may be visualised in Figure 6. In this particular case, the input parameters are represented by the letters d0 through d5, while the constant value for gene one is represented by the symbol G1c8. To facilitate the interpretation of the expression tree, a mathematical equation derived for model 3. This equation establishes a connection between the input variables and the output variables. This research analysed five independent factors and one target variable. Equation 4 as derived using just two independent variables, namely (N1)60cs and D50. This was conducted to ascertain the relationship between CRR and input components, which was derived from the Spearman's rank correlation matrix of variables shown in Figure 5.

During the process of Genetic Programming ($GP$), a multitude of potential models are created at random. Subsequently, every model undergoes training and evaluation utilising the appropriate training and testing data. Each model's fitness is evaluated by minimizing the root mean square error ($RMSE$) between the predicted and observed values of the output variable ($LI$) through the employment of the objective function ($f$).

$$RMSE = \sqrt{\frac{\sum_{i=1}^{n}(LI - LI_{Pre})^2}{n}} \quad (6)$$

Let $n$ be the total amount of incidences within the fitness group. If the errors calculated using Equation (3.1) for all models in the present population don't satisfy the termination criteria, the cycle of generating a new population continues until the desired optimal model is attained, as previously detailed.

The current study's $GP$-based model is presented in the following general manner:

$$LI_P = \sum_{i=1}^{n} F[X, f(X), C_i] + C_o \quad (7)$$

where $LI_P$ represents the predicted value of the liquefaction performance index, $F$ is the liquefaction index function created by the $GP$, $X$ is the vector of input variables, $Ci$ is a constant, $f$ represents the user-defined functions, n is the number of terms in the target expression, and $C0$ is the bias term. The $GP$, as described by Searson et al. (2010), is used in the development and implementation of the current models utilising gene expo 5.0.

After simplifying, the following algebraic equation has been obtained for CRR:

$$CRR = \tanh\left(tanh\left(\frac{1}{7.19+6.02(N_1)_{60cs}-min(3.471,(N_1)_{60cs}}\right)\right) + \frac{((N_1)_{60cs})^{\frac{1}{3}}}{2} + tan^{-1}\left(\frac{\max(D_{50},6.364)\times 3.89(N_1)_{60cs}}{4}\right) - 1.8221 \quad (8)$$

Table 3 genetic programming (GP) models

| **Model** | **Training data (in percent)** | **Testing data (in percent)** | **No. of chromosomes** | **Head size** | **No. of genes** | **Gene size** | **Program size** | **Literals** | **No. of generations** |
|---|---|---|---|---|---|---|---|---|---|
| M1 | 60 | 40 | 30 | 12 | 6 | 38 | 106 | 41 | 356684 |
| M2 | 50 | 50 | 30 | 12 | 6 | 38 | 96 | 37 | 270413 |
| M3 | 70 | 30 | 30 | 12 | 6 | 38 | 104 | 38 | 163511 |
| M4 | 80 | 20 | 30 | 12 | 6 | 38 | 104 | 40 | 260010 |
| M5 | 90 | 10 | 30 | 12 | 6 | 38 | 100 | 39 | 275015 |

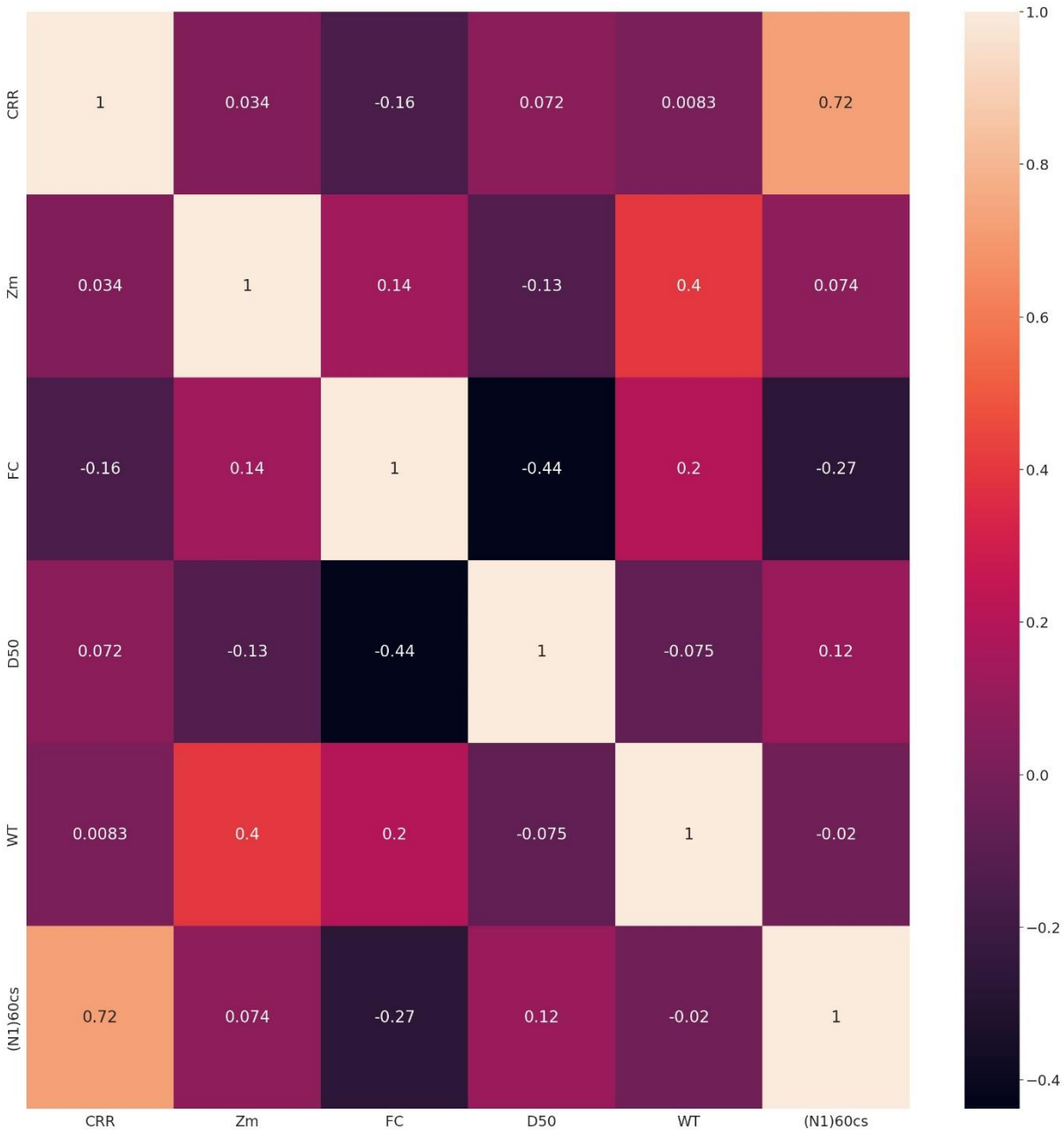


Figure 5. the Spearman's rank corelation matrix of variables used for GP

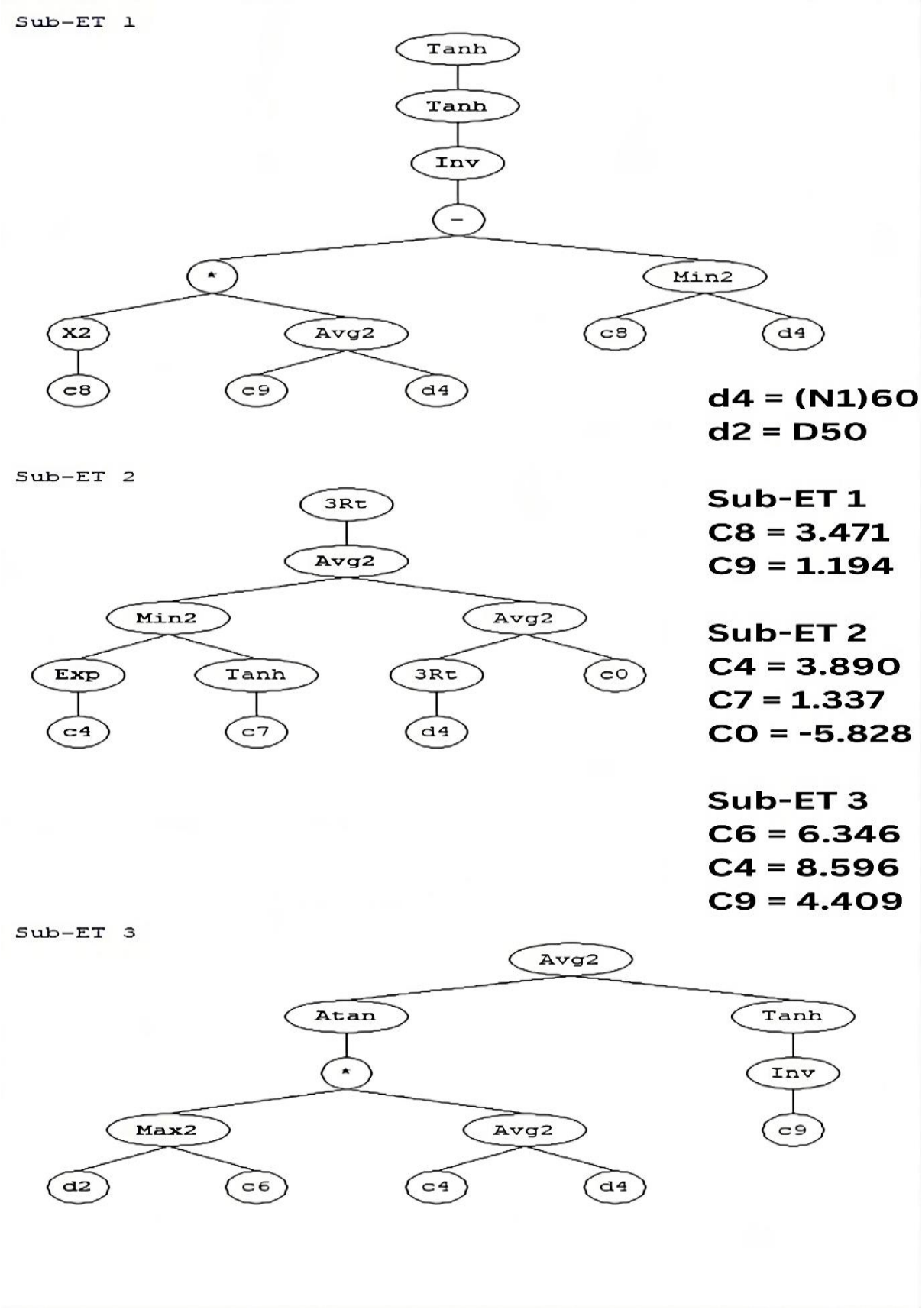


Figure 6. Expression tree for cyclic resistance ratio (CRR)

### 2.3 Probabilistic methods

Uncertainties in parameters and models make it clear that having a factor of safety (Fs) greater than 1 in liquefaction potential assessment does not provide total protection against liquefaction. Similarly, a Fs value less than or equal to 1 does not necessarily imply that liquefaction would occur. The ambiguity is resolved by taking into account the fluctuation of CRR and CSR, as seen in Figure 7. If Fs is calculated using the average values of CRR and CSR, it might exceed 1.0. Nevertheless, considering the distributions of CSR and CRR shown in Figure 7, there exists a likelihood that CRR may be lower than CSR, as indicated by the shaded area in the Figure 7, leading to Fs values below 1. This contradicts prior forecasts, in which a case originally deemed non-liquefied may ultimately be determined to be liquefied. Therefore, recent study has concentrated on evaluating the likelihood of liquefaction by estimating its probability (PL).

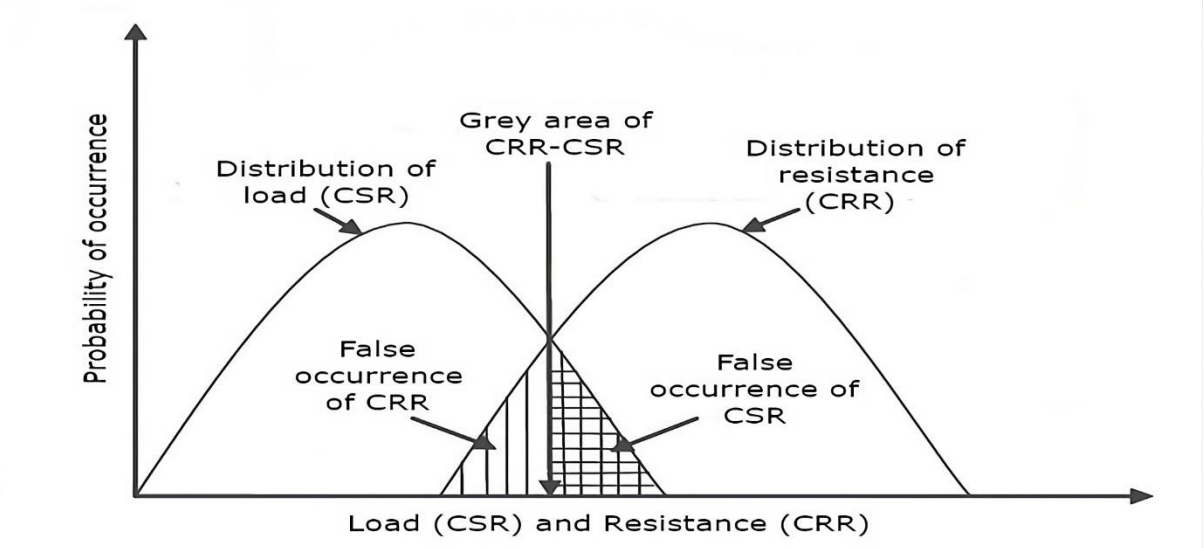


Figure 7. illustrates the prospective distribution of CRR (Cyclic Resistance Ratio) and CSR (Cyclic Stress Ratio) in the assessment of liquefaction potential

### 2.3.1 Implementation of Bayesian mapping function

Based on the research conducted by Juang et al. (1999), the probability of a case in the database undergoing liquefaction may be estimated using Bayes' theorem of conditional probability, given that the Fs has been calculated.

$$P\left(L/F_s\right) = \left(\frac{P\left(F_s/L\right)P(L)}{P\left(F_s/L\right)P(L)+P\left(F_s/NL\right)P(NL)}\right) \quad (9)$$

The equation $P\left(L/F_s\right)$ represents the probability of liquefaction given a certain value of Fs. $P\left(F_s/L\right)$ represents the probability of Fs assuming that liquefaction did occur. $P\left(F_s/NL\right)$ represents the probability of Fs assuming that liquefaction did not occur. $P(L)$ represents the prior probability of liquefaction, and $P(NL)$represents the prior probability of non-liquefaction. $P\left(F_s/L\right)$and $P\left(F_s/NL\right)$may be derived using equations (10) and (11) correspondingly.

$$P\left(F_s/L\right) = \int_{F_s}^{F_s+\Delta F_s} f_L(x)dx \quad (10)$$

$$P\left(F_s/NL\right) = \int_{F_s}^{F_s+\Delta F_s} f_{NL}(x)dx \quad (11)$$

$f_L(x)$ and $f_{NL}(x)$represent the probability density functions of Fs for examples in the database where liquefaction occurred and where liquefaction did not occur, respectively. As the change in Fs approaches zero, Equation (9) may be rewritten as Equation (12).

$$\left(L/F_s\right) = \left(\frac{f_L(F_s)P(L)}{f_L(F_s)P(L)+f_{NL}(F_s)P(NL)}\right) \quad (12)$$

Given the established prior probabilities $P(L)$ and $P(NL)$, one may use Equation (5.3) to compute the probability of liquefaction for a certain value of Fs. Without knowing the values of P(L) and P(NL), may deduce that $P(L)$ is likely to be equal to $P(NL)$ based on the principle of maximum entropy (Juang et al. 1999). Thus, if we assume that the likelihood of L is equivalent to the probability of NL, we may express Equation (12) as Equation (13).

$$P_L = \frac{f_L(F_s)}{f_L(F_s)+f_{NL}(F_s)} \quad (13)$$

The Fs values, calculated using the SPT-based deterministic approach, are computed for different cases in the collected database in this research. The examples are classified according to their observed field performance as either liquefaction (L) or non-liquefaction (NL).

Various distributions are performed for the factor of safety, and Weibull probability density function is determined to provide the most optimal fitting curves for both the L and NL groups. Figures 10 and 11 depict this. And Figure 8 and 9 shows the different percentage of each factor of safety values. The factor of safety of both groups is best described by the Weibull distribution, with scale parameter (λ) and shape parameter (k) values of 0.580 and 2.437, respectively. The probability density functions (PDF) of these Weibull distributions are seen in Figures 5.1 to 5.4 and may be expressed using Equation (14).

$$f(x;\lambda,k) = \frac{k}{\lambda}\left(\frac{x}{\lambda}\right)^{k-1} e^{-\left(\frac{x}{\lambda}\right)^{k}}, \qquad x \geq 0 \tag{14}$$

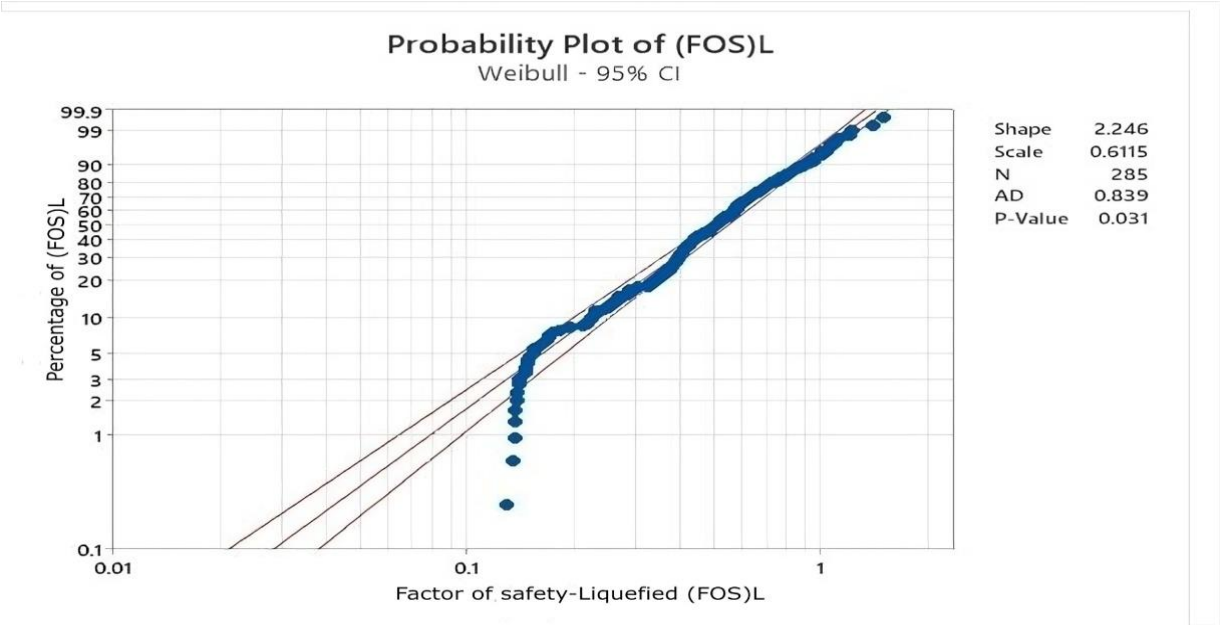


Figure 8 Percentage of probability of factor of safety liquefied data

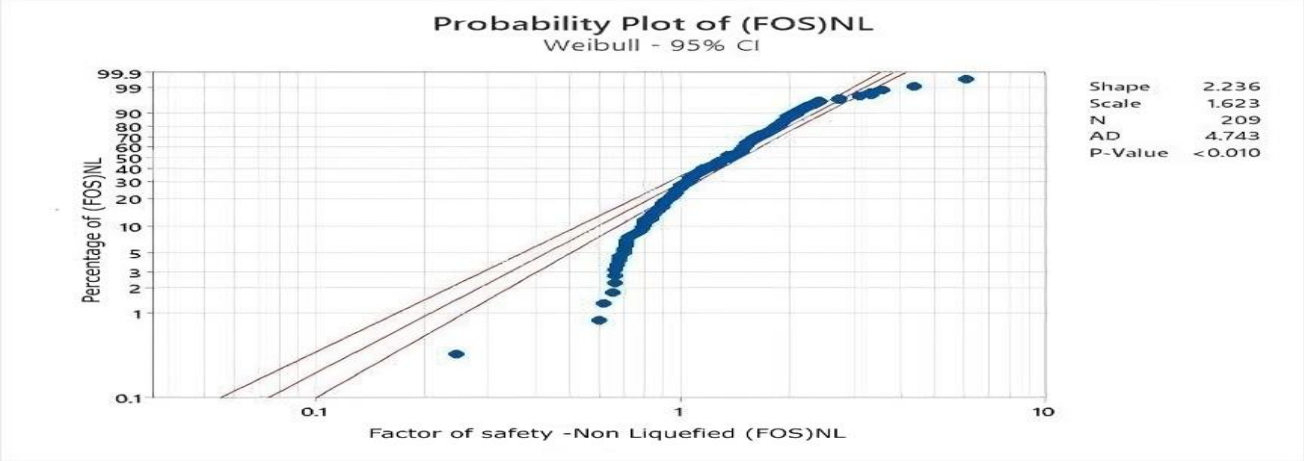


Figure 9 Percentage of probability of factor of safety non-liquefied data

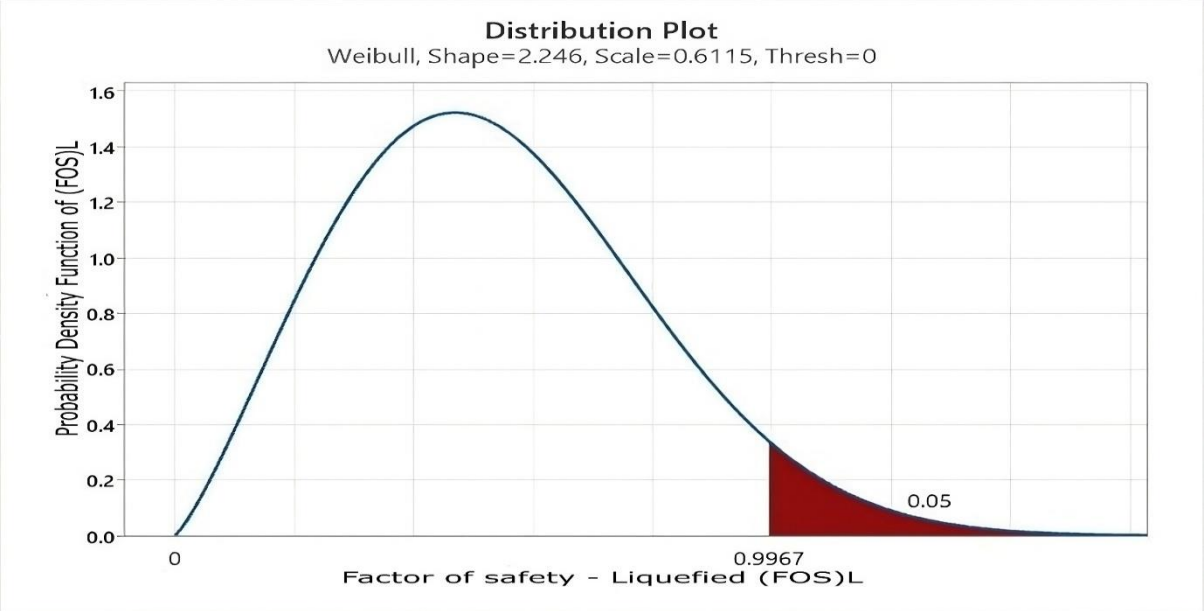


Figure 10. Weibull distribution of probability density function of liquefied data

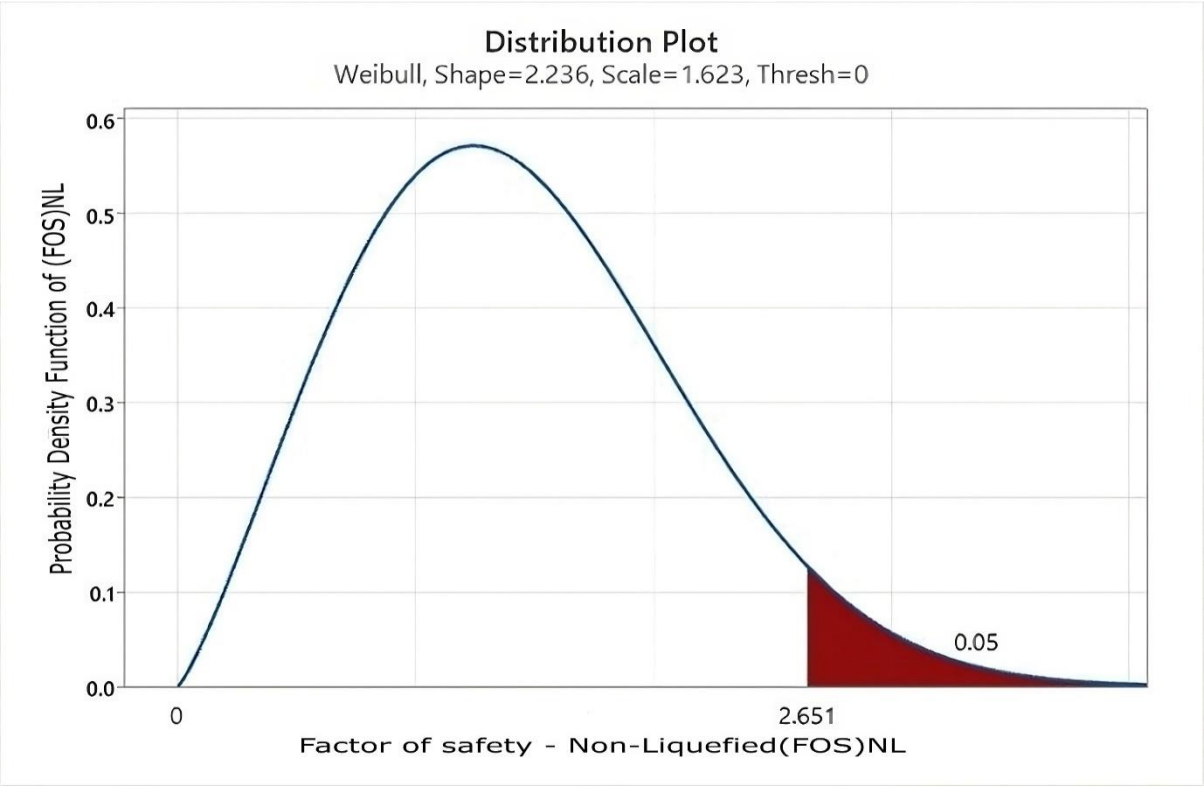


Figure 11. Weibull distribution of probability density function of non-liquefied data

## 3. Results and discussion

### 3.1 Formulation of equation by Bayesian mapping function

The probability of liquefaction ($P_L$) and probability of non-liquefaction ($P_{NL}$) for each case in the database is calculated using Equation (13), which depends on the probability density functions. The values of the factor of

safety ($Fs$) and probability of liquefaction ($P_L$) and probability of non-liquefaction ($P_{NL}$) for each of the 496 samples in the database are shown in Figure 12. A mapping function is obtained by the use of curve-fitting methodologies. The equation was formulated using the logistic curve fitting methodology. The derived equation has a coefficient of determination ($R^2$) value of 0.93. The equation (15) formulation presents the coefficients and variables, as seen in Figure 13. The derived equation is compared to the equations proposed by Toprak et al. (1999), Juang et al. (2002), and Idriss and Boulanger (2006).

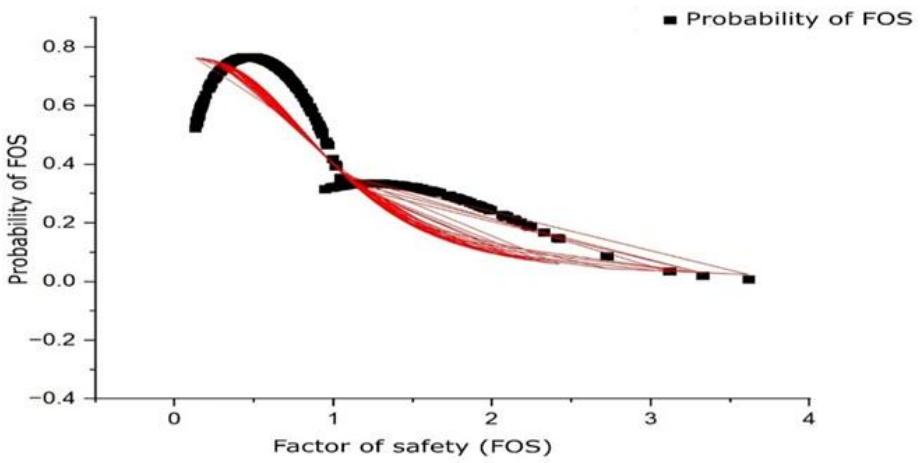


Figure 12. Curve fitting of probability of factor of safety

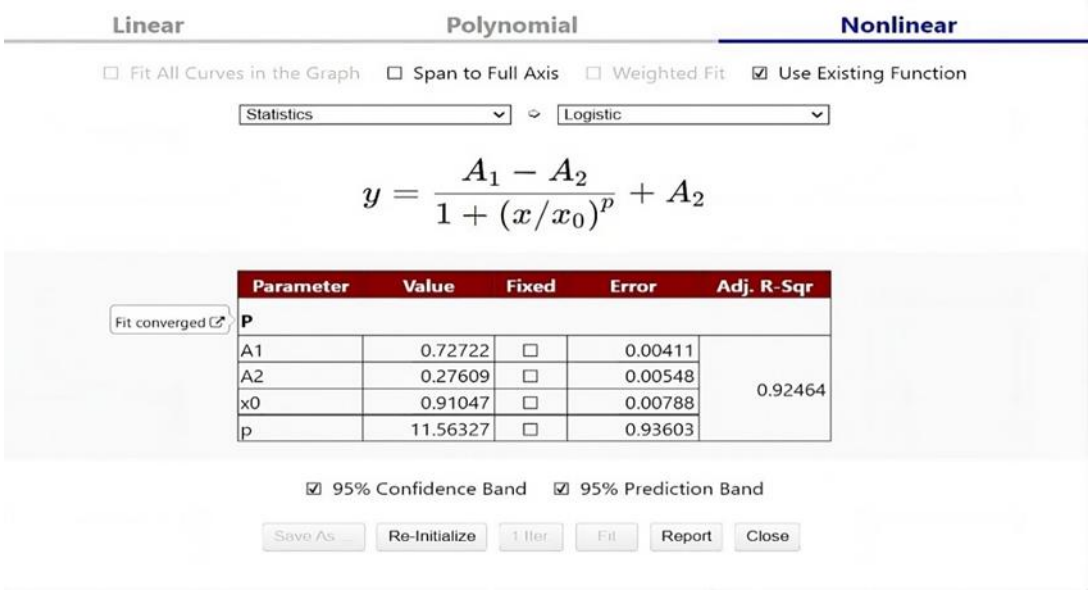


Figure 13 Curve fitting equation with constants and variables

$$P = \frac{0.45113}{1+\left(\frac{FOS}{0.91049}\right)^{11.5632}} + 0.27609 \qquad (15)$$

### 3.2 Comparison with existing methods using independent database

Regularly assessing the efficacy of a recently developed method in relation to existing methods is crucial. The present study examines the efficacy of the $GP$ −based probabilistic approach in forecasting liquefied and non-liquefied scenarios, in comparison to the equations proposed by Toprak et al. (1999), Juang et al. (2002), and Idriss & Boulanger (2006), with respect to their success rate. There are 30 databases gathered in the $NCR$ area utilizing $SPT$ tests, and these databases are used to assess the efficacy of the model.

Liquefaction probability ($P_L$) is determined by calculating its value, where a $P_L$ more than 0.5 indicates liquefied soil, while a $P_L$ less than 0.5 indicates non-liquefied soil.

Table 4 Classification criteria for liquefied and non-liquefied (Kumar et al. 2022b)

| Criteria | Probability of Liquefaction | Liquefaction Classification | Non-Liquefaction Classification |
|---|---|---|---|
| A | $P_L$> 0.85 | High Chances of Liquefaction | |
| B | $P_L$ > 0.65 | Intermediate Chances of Liquefaction | |
| C | $P_L$> 0.5 | Low Chances of Liquefaction | |
| D | $P_L$ < 0.15 | | High Chances of Non-Liquefaction |
| E | $P_L$ < 0.35 | | Intermediate Chances of Non-Liquefaction |
| F | $P_L$ < 0.5 | | Non-Low Chances of Liquefaction |

The effectiveness of the suggested techniques, based on real-world data, is assessed by calculating the probability of liquefaction using the three endorsed approaches. The present research assesses the accuracy of the suggested methods based on three criteria (A-C): High probability of liquefaction 0.85-1.0), Intermediate probability of liquefaction (0.65-1.0), and Low probability of liquefaction (0.65-1.0). The range is between 0.5 and 1.0. Criteria (D) is defined as having a high probability of non-liquefaction with a range of 0.15 to 0. Criteria (E) is defined as having an intermediate probability of non-liquefaction with a range of 0.35 to 0. Criteria (F) is defined as having a low probability of non-liquefaction with a range of 0.5 to 0. These criteria are applicable to cases when liquefaction does not occur. The categorization criteria are shown in Table 4.

### 5.5.1 Probability categorization

Table 5 Classification results of different models

| Criteria | Models | | | | | | | |
|---|---|---|---|---|---|---|---|---|
| | Proposed Model | | Toprak et al. (1999) | | Juang et al. (2002) | | Idriss and Boulanger (2006) | |
| | Count of successful prediction | Rate (%) | Count of successful prediction | Rate (%) | Count of successful prediction | Rate (%) | Count of successful prediction | Rate (%) |
| Total observed liquefied (285) | | | | | | | | |
| A ($P_L > 0.85$) | 214 | 75 | 199 | 70 | 208 | 73 | 210 | 74 |
| B ($P_L > 0.65$) | 242 | 85 | 208 | 73 | 230 | 81 | 239 | 84 |
| C ($P_L > 0.5$) | 254 | 89 | 228 | 80 | 239 | 84 | 242 | 85 |
| Total observed non-liquefied (211) | | | | | | | | |
| D ($P_L < 0.15$) | 127 | 60 | 65 | 31 | 105 | 50 | 91 | 43 |
| E ($P_L < 0.35$) | 137 | 65 | 89 | 42 | 120 | 57 | 108 | 51 |
| F ($P_L < 0.5$) | 154 | 73 | 120 | 57 | 139 | 66 | 129 | 61 |

The results are shown in Table 5 , which classifies the soil that has the potential to liquefy (Criteria A-C) and the soil that does not have the potential to liquefy (Criteria D-F) based on the predictive accuracy of each recommended approach.

The findings from Table 5 show that the Proposed Model, which is based on certain criteria, has a higher success rate in predicting liquefaction cases compared to the models developed by Idriss & Boulanger (2006), Juang et al. (2002), and Toprak et al. (1999). Specifically, the Proposed Model achieved success rates of 75% for A, 85% for B, and 89% for C, whereas the other models achieved lower success rates ranging from 70% to 84%. Furthermore, compared to Idriss & Boulanger (2006) (A = 74%, B = 84% and C= 85%), Juang et al. (2002) (A = 73%, B = 81% and C= 84%) And Toprak et al. (1999) (A = 70%, B = 73% and C= 80%) proposed model has a greater success rate of non-liquefiable case prediction.

### 5.5.2 Performance fitness and error metrics (PFEMs)

Table 6 Comparative analysis of the proposed approach with existing techniques for binary classification

| Matrices | Models | | | | |
|---|---|---|---|---|---|
| | Proposed Model | Toprak et al. (1999) | Juang et al. (2002) | Idriss and Boulanger (2006) | Range |
| TPR | 0.89 | 0.762 | 0.84 | 0.85 | 1.0 |
| FNR | 0.108 | 0.237 | 0.161 | 0.15 | 0.0 |
| PPV/Precision | 0.817 | 0.714 | 0.768 | 0.746 | 1.0 |

| | | | | | |
|---|---|---|---|---|---|
| NPV | 0.832 | 0.628 | 0.751 | 0.75 | 1.0 |
| FPR | 0.270 | 0.431 | 0.341 | 0.388 | 0.0 |
| FDR | 0.183 | 0.285 | 0.231 | 0.253 | 0.0 |
| FOR | 0.168 | 0.372 | 0.249 | 0.25 | 0.0 |
| $F_1$ Score | 0.852 | 0.737 | 0.802 | 0.794 | 1.0 |
| MCC | 0.634 | 0.3851 | 0.508 | 0.478 | -1.0 to + 1.0 |
| Accuracy | 0.822 | 0.682 | 0.762 | 0.747 | 1.0 |
| Sensitivity/Recall | 0.891 | 0.762 | 0.838 | 0.849 | 1.0 |
| Specificity | 0.729 | 0.568 | 0.658 | 0.611 | --------- |
| G $_{\text{mean error}}$ | 0.193 | 0.342 | 0.257 | 0.279 | 0.0 |
| BA | 0.81 | 0.665 | 0.748 | 0.730 | 1.0 |

Utilising Performance Fitness and Error Metrics ($PFEMs$) for binary classification. In order to fully evaluate the efficacy of the proposed approaches for classifying liquefaction problems, several Performance Fitness and Error Metrics ($PFEMs$) are used in this section. Within the binary classification scenario, including both liquefied and non-liquefied instances, there are four distinct possible outcomes for a single prediction. The terms "true negative" ($TN$) and "true positive" ($TP$) refer to accurate classifications. A false positive ($FP$) occurs when the output is erroneously predicted to be negative, whereas a false negative ($FN$) arises when the outcome is mistakenly classified as negative. The 2 × 2 confusion matrix seen in Figure 5.7 may be used to assess these matrices. $PFEMs$ are used to elucidate the correspondence between probabilistic forecasts of suggested methodologies and the actual outcome. These measures often pertain to the discrepancy in variance between the predicted and actual data. In this study, we used specific Performance Fitness and Error Metrics ($PFEMs$) to evaluate categorization issues (Naser and Alavi 2021). The mathematical representation of these $PFEMs$ is provided below:

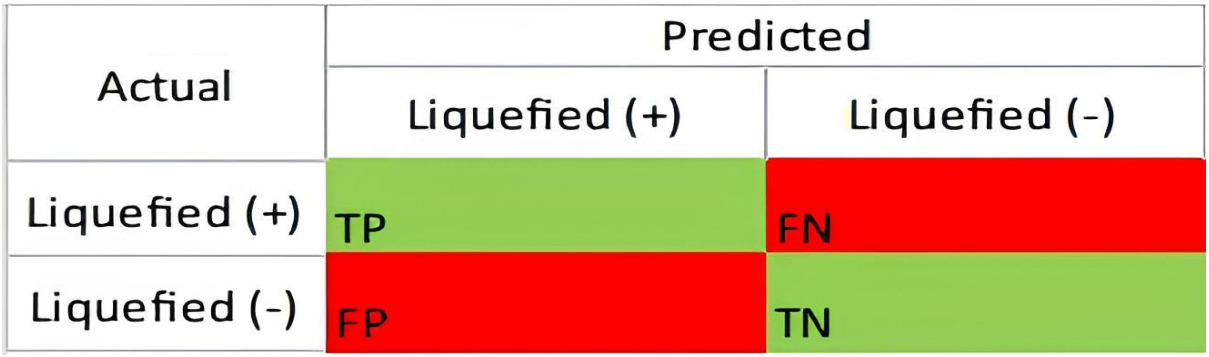


Figure 14 Illustration of confusion matrix (2 × 2) for classification problem

$$TPR = \frac{TP}{TP+FN} \tag{5.7}$$

$$FNR = \frac{FN}{FN+TP} \tag{5.8}$$

$$PPV = \frac{TP}{TP+FP} \quad (5.9)$$

$$NPV = \frac{TN}{TN+FN} \quad (5.10)$$

$$FPR = \frac{FP}{FP+TN} \quad (5.11)$$

$$FDR = \frac{FP}{FP+TP} \quad (5.12)$$

$$FOR = \frac{FN}{FN+TP} = 1 - NPV \quad (5.13)$$

$$F_{1\,SCORE} = \frac{2TP}{2TP+FP+FN} \quad (5.14)$$

$$MCC = \frac{TP \times TN - FP \times FN}{\sqrt{(TP+FP)(TP+FN)(TN+FP)(TN+PN)}} \quad (5.15)$$

$$Accuracy = \frac{TP+TN}{FN+TP+FP+TN} \quad (5.16)$$

$$Sensitivity = \frac{TP}{FN+TP} \quad (5.17)$$

$$Specificity = \frac{TN}{FP+TN} \quad (5.18)$$

$$G_{(mean)error} = 1 - \sqrt{Sensitivity \times Specificity} \quad (5.19)$$

$$BA = 0.5 \times \left(\frac{TP}{TP+FN} + \frac{TN}{TN+FP}\right) \quad (5.20)$$

Table 7 Score analysis of the proposed method and existing methods

| Matrices | Proposed Model | Toprak et al. (1999) | Juang et al. (2002) | Idriss and Boulanger (2006) |
|---|---|---|---|---|
| TPR | 4 | 1 | 2 | 3 |
| FNR | 4 | 1 | 2 | 3 |
| PPV | 4 | 1 | 3 | 2 |
| NPV | 4 | 1 | 3 | 2 |
| FPR | 4 | 1 | 3 | 2 |
| FDR | 4 | 1 | 3 | 2 |
| FOR | 4 | 1 | 3 | 2 |
| $F_1$ Score | 4 | 1 | 3 | 2 |
| MCC | 4 | 1 | 3 | 2 |
| Accuracy | 4 | 1 | 3 | 2 |
| Sensitivity | 4 | 1 | 2 | 3 |
| Specificity | 4 | 1 | 3 | 2 |
| $G_{\text{mean error}}$ | 4 | 1 | 3 | 2 |

| | | | | |
|---|---|---|---|---|
| BA | 4 | 1 | 3 | 2 |
| Total Score | 56 | 14 | 39 | 31 |
| Rank | 1 | 4 | 2 | 3 |

Within this particular framework, $TP$ denotes the count of positive examples that were accurately assigned to their respective categories, $TN$ denotes the count of negative instances that were correctly classified, $FN$ denotes the count of positive instances that were erroneously classified, and $FP$ denotes the count of negative instances that were inaccurately classified. The binary classification predictions and actual observations were compared by analysing the $PFEMs$ data shown in Table 6.

The true positive rate ($TPR$) measures the ratio of accurately detected positive cases to the total number of actual positive cases. This exercise does not consider indeterminate outcomes. The $TPR$ values of the suggested model (0.89) were found to be higher than those of the Idriss and Boulanger (2006) (0.85), Toprak et al. (1999) (0.762), and Juang et al. (2002) (0.84) approaches. The positive predictive value (PPV) is a measure that represents the percentage of positive observations that actually result in true positive values. The PPV value obtained for the proposed model (0.817) is higher than the values obtained by Juang et al. (2002) (0.764), Idriss and Boulanger (2006) (0.746), and Toprak et al. (1999) (0.714) techniques. The optimal and suboptimal values for the Negative Predictive Value ($NPV$) are 1 and 0, correspondingly. It computes the ratio of incorrect positive results among observations that seem to be negative. The suggested model (0.832) outperforms the Juang et al. (2002) (0.751), Idriss and Boulanger (2006) (0.75), and Toprak et al. (1999) (0.628) approaches. A perfect prediction accuracy would include a False Positive Rate ($FPR$) of zero, indicating that no negative instances are incorrectly categorised as positive ones. Although the FPR score of the suggested model (0.270) is lower than that of Juang et al. (2002) (0.341), Idriss and Boulanger (2006) (0.388), and Toprak et al. (1999) (0.431) approaches. The False Discovery Rate ($FDR$) refers to the proportion of individuals who have a positive test result while not having the real ailment. The false discovery rate (FDR) obtained in this study for the proposed model (0.183) is lower than that reported by Juang et al. (2002) (0.231), Idriss and Boulanger (2006) (0.253), and Toprak et al. (1999) (0.285). This indicates that the proposed method outperformed the methods employed by Idriss and Boulanger (2006), Toprak et al. (1999), and Juang et al.

The False Omission Rate ($FOR$) quantifies the proportion of individuals whose test results indicated a negative outcome, although really having a positive condition. The suggested technique (0.168) has a lower value compared to the procedures used by Toprak et al. (1999) (0.372), Juang et al. (2002) (0.249), and Idriss and Boulanger (2006) (0.25). The suggested approaches' accuracy is evaluated using the F1 score. The $F1$-score obtained for the suggested approach (0.852) is greater than that for the Idriss and Boulanger (0.794), Toprak et al. (1999) (0.737), and Juang et al. (2002) methodologies. This indicates that the proposed method is more accurate in forecasting the possibility of liquefaction. Furthermore, the assessment of a binary classifier's effectiveness involves the use of Balanced Accuracy ($BA$), miss or false negative rate (FNR), $Gmean$ error, and the Matthews correlation coefficient (MCC). The definitions of balanced accuracy and G(mean) error may be found in Equation (5.17) and Equation (5.19) accordingly. The miss rate indicates the quantity of liquefied or non-liquefied substances that could have been incorrectly classified as not having the potential to cause tsunamis. $Gmean$ is often used when each class's performance is both remarkable and anticipated to be excellent simultaneously (Kubat and Matwin

1997; Yuan and Liu 2011). The given value is the geometric mean of the correctness of each instance inside each class. To assess the efficacy of the classifier model, some studies have used $Gmean$ as a measure of error rate, in addition to the $F1$-score. Matthews (1975) established the Matthews Correlation Coefficient ($MCC$) to measure the effectiveness of a model when there is a significant difference between the percentage of positive and negative data. The $MCC$ is particularly valuable in such scenarios. The MCC value must fall between the range of -1.0 and +1.0. Conversely, a preference for the greater number indicates a more accurate forecast.

When compared to the criteria established by Toprak et al. (1999) (0.385), Juang et al. (2002) (0.508), and Idriss and Boulanger (2006) (0.478), the suggested method's MCC value (0.634) indicates that it outperforms these criteria in predicting liquefaction likelihood. The False Negative Rate (FNR) accurately predicts cases of liquefaction turning into non-liquefaction. $FNR$ provides a clearer understanding of where sudden failure occurs. In this study, the proposed method (0.108) demonstrates lower FNR values compared to Toprak et al. (1999) (0.237), Juang et al. (2002) (0.161), and Idriss and Boulanger (2006) (0.15). Score analysis is performed to assess the effectiveness of the suggested methods. The score is calculated for each strategy by considering their performance fitness and error matrices. The score value range is defined by the total number of approaches used in this study, which is 1-4 (with a total of 4 procedures applied). The score value in this study is calculated based on the obtained value of PFEMs. The procedures that possess the most worth for any particular $PFEMs$, with an optimal value of 1.0, are assigned a maximum score of 4.0. On the other hand, the methods that have the greatest significance for any particular PFEMs with an optimal value of 0.0 are assigned a minimum score of 0. The proposed methodology in this research has received the highest score of 56, as shown in Table 7. Thus, the suggested approach has obtained the highest ranking, with Juang et al. (2002), Idriss and Boulanger (2006), and Toprak et al. (1999) methods following in subsequent positions. Scatter plots are shown for both liquefied and non-liquefied samples, demonstrating all the recommended methods for the parameters $(N1)$,$60cs$, and $CSR$. The scatter plots in Figures 15, 16, 17, and 18 illustrate the correlation between the total number of liquefied and non-liquefied instances for the Proposed Model, Toprak et al. (1999), Idriss and Boulanger (2006), and Juang et al. (2002) techniques. These charts illustrate the comparison between the observed and forecasted values. The scatter plot of the Proposed Model exhibits distinct and improved segregation, aligning closely with the projected value ranges in contrast to the other models. Conversely, the scatter plot for Toprak et al. (1999) demonstrates a substantial degree of inaccuracy in forecasting both liquefied and non-liquefied instances.

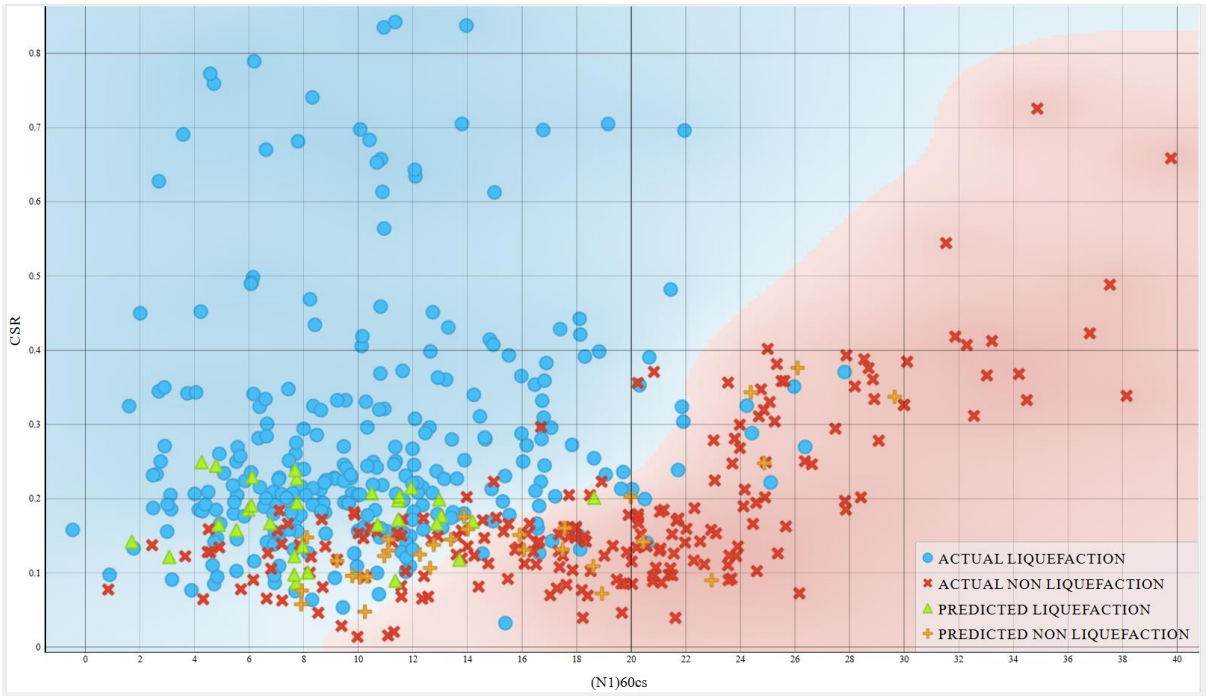


Figure 15 Visualisation of observed and forecasted instances using the suggested methodology

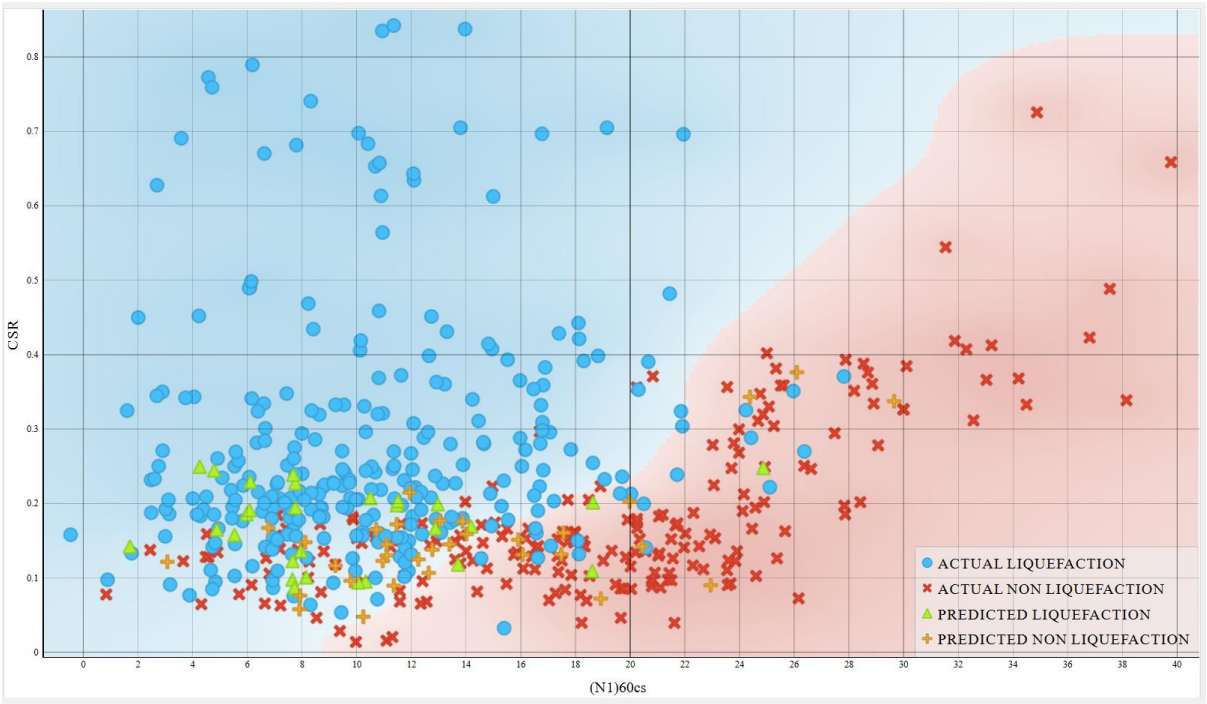


Figure 16 Visualisation of observed and forecasted instances of Juang et al. (2002) method

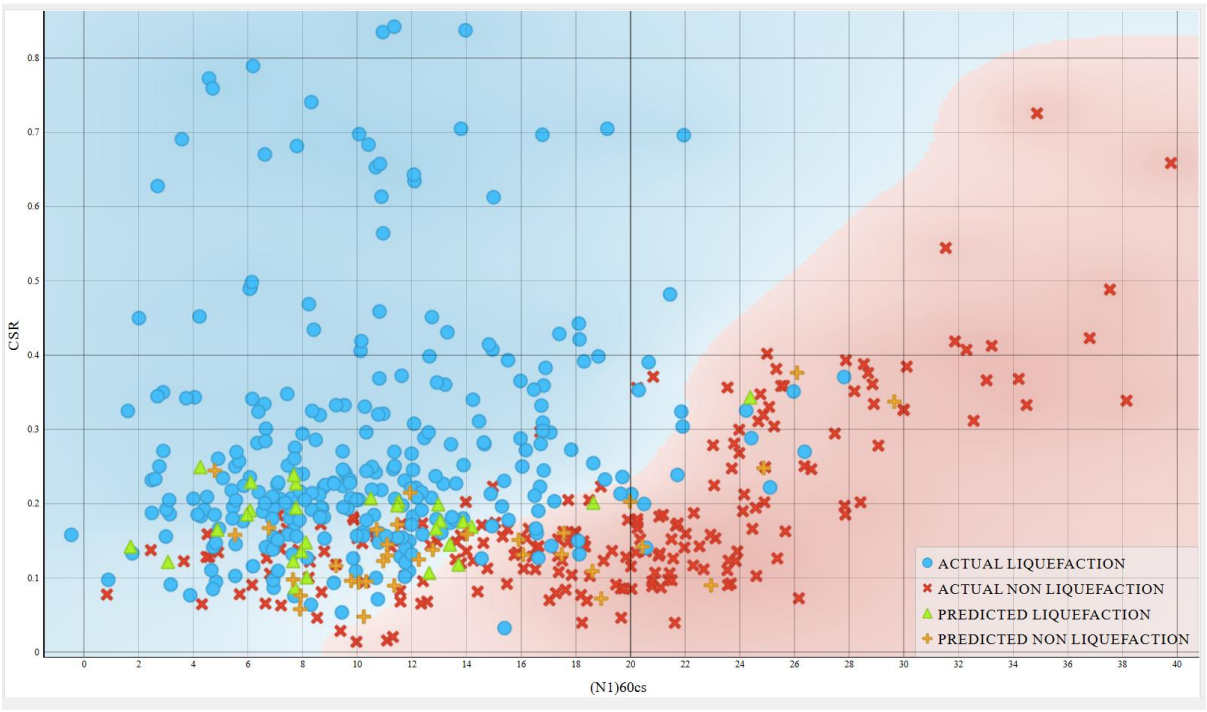


Figure 17 Visualisation of observed and forecasted instances of Idriss and Boulanger (2006) method

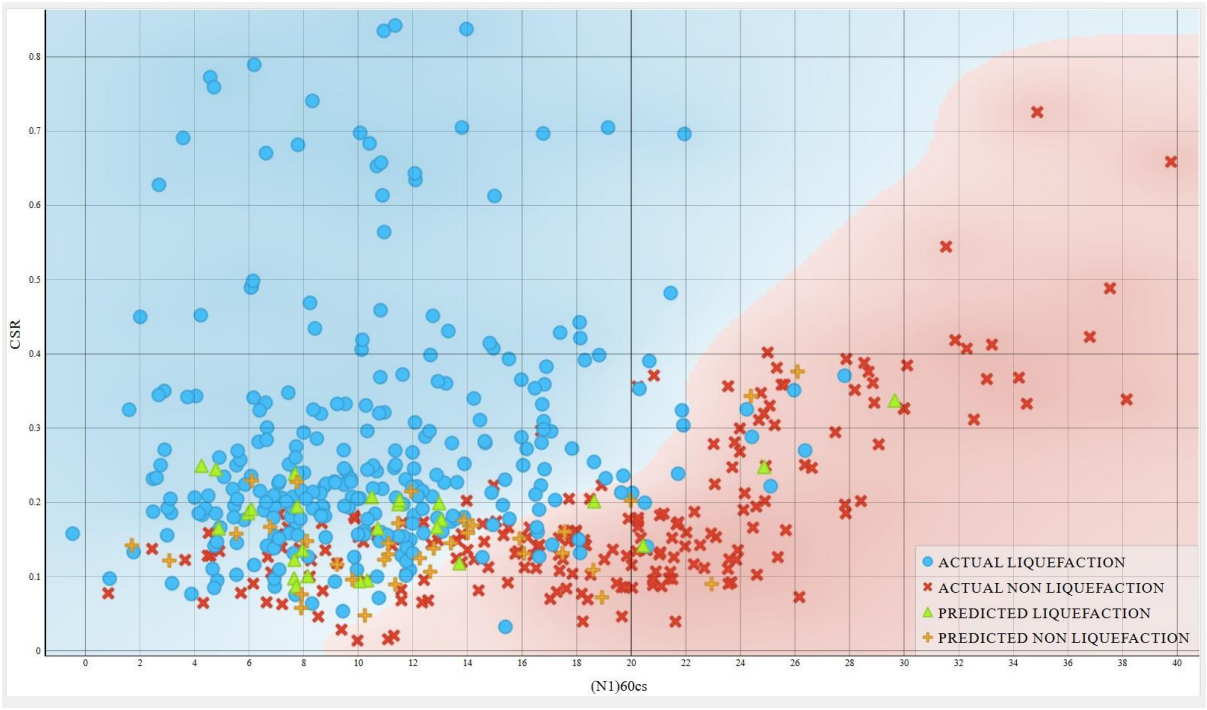


Figure 18 Visualisation of observed and forecasted instances of Toprak et al. (1999) method

### 3.3 Evaluating the proportional impact of various criteria on the computation of PL using the Gini Index (GI)

The Gini index ($GI$) is used to evaluate the relative significance of independent variables in predicting the likelihood of soil deposit liquefaction. The Gini index has been computed for each independent variable, and their relative significance has been evaluated. A higher Gini index value signifies a stronger influence of individual independent elements in forecasting the likelihood of soil liquefaction in a deposit. The Gini index is calculated using the following mathematical equation:

$$GI = \left|\sum_{i=2}^{n} Cum\ X_{i-1} Cum\ P_{Li} - \sum_{i=2}^{n} Cum\ X_i Cum\ P_{Li-1}\right| \qquad (5.21)$$

Here, $CumX$ denotes the cumulative value of independent variables, whereas CumPL represents the cumulative value of liquefaction probability for a set of $n$ observed data points. The Gini index values for all three approaches, considering various input variables such as Critical depth, $FC, D50, PGA, rd,$ Water Table $(W.T), CSR$, and $(N1)60CS$, are shown in Table 5.5.

The results shown in Table 8 demonstrate that the Gini index value for each independent variable in the proposed technique is lower than the values obtained in the methods used by Juang et al. (2002), Toprak et al. (1999), and Idriss and Boulanger (2006). These findings indicate that each component has a substantial impact on the capacity to estimate the likelihood of liquefaction using the suggested approach.

Table 8 Gini index value for all proposed and existing methods

| Variables | Proposed Model | Toprak et al. (1999) | Juang et al. (2002) | Idriss and Boulanger (2006) |
|---|---|---|---|---|
| Critical depth | 150.763 | 208.26 | 593.07 | 553.543 |
| FC | 336.26 | 314.6 | 979.8 | 811.6 |
| D50 | 3.1259 | 4.7289 | 18.6078 | 17.0856 |
| Water Table | 140.165 | 177.05 | 296.85 | 288.44 |
| PGA | 2.56265 | 4.3765 | 22.9305 | 20.828 |
| rd | 34.0271 | 37.116 | 18.033 | 10.0435 |
| CSR | 1.85031 | 1.0921 | 7.4296 | 13.1889 |
| $(N_1)_{60CS}$ | 1849.761 | 2180.662 | 1523.244 | 1678.829 |

**4. conclusions**

The study attempts to develop a probabilistic liquefaction method using updated cyclic resistance ratio (CRR) and cyclic stress ratio (CSR) by the application of Bayes' conditional probability theorem. The study used a dataset that included several instances of post-liquefaction occurrences, including the time period from the 1944 Tohnankai earthquake to the 1999 Chi Chi earthquake in Taiwan. The dataset included 286 occurrences of liquefaction and 210 occurrences of non-liquefaction. Furthermore, a set of 30 borehole data obtained from the Standard Penetration Test (SPT) were collected in the Faridabad area, which is situated in the National Capital area (NCR) of Delhi, India. These acquired 30 borehole data were used to verify the accuracy of both the proposed and current models.

(1) Data visualization is essential for improving comprehension of data patterns, the relationships and distinctions among several variables used in research, and the level of disorder or unpredictability inherent in the data. The correlation coefficient between (PGA) and (CSR) is 0.89, indicating a strong positive link. Similarly, there is a strong negative correlation of -0.97 between the overburden correction factor (rd) and critical depth. Based on theoretical research, it is essential to eliminate one of these aspects from each combination. However, this study acknowledges the importance of both variables and acknowledges their distinct contributions to the analysis of liquefaction studies.

(2) The analysis of entropy reveals, via the use of pair plots, a significant lack of clear separation between the two data groups, hence indicating a substantial level of complexity. Thus, the analysis of complex datasets may require more sophisticated models to address this complex problem, it is recommended to use advanced techniques like Genetic Programming (GP) and advanced deep learning models to get improved results.

(3) Through the use of variables, the present work used genetic programming (GP) to produce several models, each characterized by unique combinations of training and testing datasets, program dimensions, and generations. The current investigation used the root-mean-squared error (RMSE) as the fitness function, and the measure of fitness was obtained by using an equation formed from the expression tree. The expression tree generated by the GP model 3 resulted in a mathematical equation that demonstrated improved performance for the input and output variables.

(4) After formulating the new equation for cyclic resistance ratio (CRR), the factor of safety (Fs) has been determined by using the new CRR equation and cyclic stress ratio (CSR). Subsequently, several probability density functions are applied to the calculated factor of safety. It has been observed that the Weibull probability density functions provide the most accurate fitting curves for both liquefied (L) and non-liquefied (NL) conditions.

(5) The probability of the liquefied equation was determined by using probability density curves and the Bayes' conditional probability theorem. The values derived from the Bayes' conditional probability theorem were further used in logistic curve fitting to formulate an equation, which was further compared to pre-existing probabilistic models. A comparison was made between the novel methodology and the techniques proposed by Juang et al. (2002), Toprak et al. (1999), and Idriss and Boulanger (2006). The comparison included employing a confusion matrix for binary classification and doing a score analysis based on factor ranking. The proposed model exhibited superior performance, as the outputs of the constructed model increased for all positive factors and decreased for negative indicators.

(6) The Gini index was finally calculated for the proposed method and the existing methods by Juang et al. (2002), Toprak et al. (1999), and Idriss and Boulanger (2006). It was observed that all the existing methods were biased towards a limited number of variables. However, the proposed method demonstrated the significance of all variables in predicting the probability of liquefaction.

**References**

Addo, K. O., & Robertson, P. K. (1992). Shear-wave velocity measurement of soils using Rayleigh waves. *Canadian Geotechnical Journal*, 29(4), 558-568.

Andrus, R. D., & Stokoe II, K. H. (2000). Liquefaction resistance of soils from shear-wave velocity. Journal of geotechnical and geoenvironmental engineering, 126(11), 1015-1025.

Andrus, R. D., Stokoe, K. H., & Hsein Juang, C. (2004). Guide for shear-wave-based liquefaction potential evaluation. Earthquake Spectra, 20(2), 285-308.

Baziar, M. H., & Jafarian, Y. (2007). Assessment of liquefaction triggering using strain energy concept and ANN model: capacity energy. *Soil Dynamics and Earthquake Engineering*, 27(12), 1056-1072.

Becker, D. E. (1997). Eighteenth Canadian geotechnical colloquium: Limit states design for foundations. Part I. An overview of the foundation design process. *Canadian Geotechnical Journal*, *33*(6), 956-983.

Boulanger, R. W., & Idriss, I. M. (2014). CPT and SPT based liquefaction triggering procedures. Report No. UCD/CGM.-14, 1.

Cetin, K. O., and Seed, R. B. (2004). "Nonlinear shear mass participation factor (rd) for cyclic shear stress ratio evaluation." *Soil Dynamics and Earthquake Engineering*, Elsevier, 24: 103-113.

Ferreira, C. (2002). Gene expression programming in problem solving. In *Soft computing and industry: recent applications* (pp. 635-653). London: Springer London.

Goh, A. T. (1994). Seismic liquefaction potential assessed by neural networks. Journal of Geotechnical engineering, 120(9), 1467-1480.

Goharzay, M., Noorzad, A., Ardakani, A. M., & Jalal, M. (2017). A worldwide SPT-based soil liquefaction triggering analysis utilizing gene expression programming and Bayesian probabilistic method. Journal of Rock Mechanics and Geotechnical Engineering, 9(4), 683-693.

Haldar, A., & Tang, W. H. (1979). Probabilistic evaluation of liquefaction potential. Journal of the Geotechnical Engineering Division, 105(2), 145-163.

Hanna, A. M., Ural, D., & Saygili, G. (2007). Evaluation of liquefaction potential of soil deposits using artificial neural networks. Engineering Computations, 24(1), 5-16.

Harder, L. F., & Seed, H. B. (1986). Determination of penetration resistance for coarse-grained soils using the Becker hammer drill. Berkeley, CA, USA: College of Engineering, University of California.

Hu J, Liu H (2019) Bayesian network models for probabilistic evaluation of earthquake-induced liquefaction based on CPT and Vs databases. Eng Geol 254:76–88.

Hu J (2021a) A new approach for constructing two Bayesian network models for predicting the liquefaction of gravelly soil. *Comput Geotech* 137:104304.

Hu, J. (2021b). Data cleaning and feature selection for gravelly soil liquefaction. *Soil Dynamics and Earthquake Engineering*, *145*, 106711.

Hu J, Wang J, Zhang Z, Liu H (2022) Continuous-discrete hybrid Bayesian network models for predicting earthquake-induced liquefaction based on the Vs database. *Comput Geosci* 169:105231.

Idriss, I. M., and Boulanger, R. W. (2004). Semi-empirical procedures for evaluating liquefaction potential during earthquakes, in Proceedings, *11th International Conference on Soil Dynamics and Earthquake Engineering, and 3rd International Conference on Earthquake Geotechnical Engineering,* D. Doolin et al., eds., Stallion Press, Vol. 1, pp. 32–56.

Idriss, I. M., and Boulanger, R. W. (2006). Semi-empirical procedures for evaluating liquefaction potential during earthquakes, *J. Soil Dynamics and Earthquake* Eng. 26, 115–30.

Idriss, I. M., and Boulanger, R. W. (2008). Soil liquefaction during earthquakes. Monograph MNO-12, Earthquake Engineering Research Institute, Oakland, CA, 261 pp.

Idriss IM, Boulanger RW (2010) Spt-based liquefaction triggering procedures. Rep. UCD/CGM-10. 2, 4–13.

Jas, K., & Dodagoudar, G. R. (2023). Explainable machine learning model for liquefaction potential assessment of soils using XGBoost-SHAP. *Soil Dynamics and Earthquake Engineering*, *165*, 107662.

Juang, C. H., Rosowsky, D. V., & Tang, W. H. (1999). Reliability-based method for assessing liquefaction potential of soils. *Journal of Geotechnical and Geoenvironmental Engineering*, 125(8), 684-689.

Juang, C. H., Chen, C. J., Jiang, T., & Andrus, R. D. (2000). Risk-based liquefaction potential evaluation using standard penetration tests. Canadian Geotechnical Journal, 37(6), 1195-1208.

Juang, C. H., Chen, C. J., & Jiang, T. (2001). Probabilistic framework for liquefaction potential by shear wave velocity. *Journal of geotechnical and geoenvironmental engineering*, 127(8), 670-678.

Juang CH, Jiang T, Andrus RD (2002) Assessing probability-based methods for liquefaction potential evaluation. J Geotech Geoenviron Eng 128:580–589

Juang, C. H., Fang, S. Y., & Khor, E. H. (2006). First-order reliability method for probabilistic liquefaction triggering analysis using CPT. *Journal of Geotechnical and Geoenvironmental Engineering*, 132(3), 337-350.

Kayen, R. E., Mitchell, J. K., Seed, R. B., Lodge, A., Nishio, S. Y., & Coutinho, R. (1992, May). Evaluation of SPT-, CPT-, and shear wave-based methods for liquefaction potential assessment using Loma Prieta data. *In Proceedings of the 4th Japan-US Workshop on Earthquake Resistant Design of Lifeline Facilities and Countermeasures for Soil Liquefaction*, Hamada, M. and O'Rourke, TD, eds.

Kohestani, V. R., Hassanlourad, M., & Ardakani, A. J. N. H. (2015). Evaluation of liquefaction potential based on CPT data using random forest. Natural Hazards, 79(2), 1079-1089.

Kumar, D. R., Samui, P., & Burman, A. (2022a). Prediction of probability of liquefaction using soft computing techniques. *Journal of The Institution of Engineers* (India): Series A, 103(4), 1195-1208.

Kumar, D. R., Samui, P., & Burman, A. (2022b). Determination of best criteria for evaluation of liquefaction potential of soil. Transportation Infrastructure Geotechnology, 1-20.

Liao, S. S., Veneziano, D., & Whitman, R. V. (1988). Regression models for evaluating liquefaction probability. *Journal of Geotechnical Engineering*, 114(4), 389-411.

Mitchell, J. K., & Tseng, D. J. (1990, May). Assessment of liquefaction potential by cone penetration resistance. In Proc., H. Bolton Seed Memorial Symp. Duncan (pp. 335-350). Vancouver, Canada: JM BiTech.

Momeni, E., Armaghani, D. J., Hajihassani, M., & Amin, M. F. M. (2015). Prediction of uniaxial compressive strength of rock samples using hybrid particle swarm optimization-based artificial neural networks. Measurement, 60, 50-63.

Muduli, P. K., & Das, S. K. (2015). First-order reliability method for probabilistic evaluation of liquefaction potential of soil using genetic programming. *International Journal of Geomechanics,* 15(3), 04014052.

National Research Council (NRC) (1985). Liquefaction of Soils During Earthquakes, National Academy Press, Washington, DC, 240 pp.

Naser, M. Z., & Alavi, A. H. (2021). Error metrics and performance fitness indicators for artificial intelligence and machine learning in engineering and sciences. *Architecture, Structures and Construction*, 1-19.

Oliveira, L. O. V., Otero, F. E., & Pappa, G. L. (2016, July). A dispersion operator for geometric semantic genetic programming. In *Proceedings of the Genetic and Evolutionary Computation Conference 2016* (pp. 773-780).

Olsen, R. S. (1988, June). Using the CPT for dynamic site response characterization. In Earthquake Engineering and Soil Dynamics II—Recent Advances in Ground-Motion Evaluation (pp. 374-388). ASCE.

Olsen, R. S. (1997, December). Cyclic liquefaction based on the cone penetrometer test. In Proceedings of *the NCEER Workshop on Evaluation of Liquefaction Resistance of Soils* (pp. 225-276). Buffalo: State University of New York.

Pal, M. (2006). Support vector machines-based modelling of seismic liquefaction potential. *International Journal for Numerical and Analytical Methods in Geomechanics*, 30(10), 983-996.

Pirhadi N,Wan X, Lu J, Hu J, AhmadM, Tahmoorian F (2023) Seismic liquefaction resistance based on strain energy concept considering fine content value effect and performance parametric sensitivity analysis. C Model Eng Sci 135:733–754.
Ramakrishnan, D., Singh, T. N., Purwar, N., Barde, K. S., Gulati, A., & Gupta, S. (2008). Artificial neural network and liquefaction susceptibility assessment: a case study using the 2001 Bhuj earthquake data, Gujarat, India. *Computational Geosciences*, 12, 491-501.

Robertson, P. K., & Campanella, R. G. (1985). Liquefaction potential of sands using the CPT. Journal of geotechnical engineering, 111(3), 384-403.

Robertson, P. K., & Wride, C. E. (1998). Evaluating cyclic liquefaction potential using the cone penetration test. *Canadian geotechnical journal*, 35(3), 442-459.

Samui, P., & Hariharan, R. (2015). A unified classification model for modeling of seismic liquefaction potential of soil based on CPT. *Journal of advanced research*, 6(4), 587-592.

Samui, P., & Karthikeyan, J. (2013). Determination of liquefaction susceptibility of soil: a least square support vector machine approach. International Journal for Numerical and Analytical Methods in Geomechanics, 37(9), 1154-1161.

Samui, P., & Sitharam, T. G. (2011). Machine learning modelling for predicting soil liquefaction susceptibility. *Natural Hazards and Earth System Sciences*, 11(1), 1-9.

Seed, H. B., and Idriss, I. M. (1967). "Analysis of liquefaction: Niigata earthquake." Proc., ASCE, 93(SM3), 83-108.

Seed, H. B., & Idriss, I. M. (1971). Simplified procedure for evaluating soil liquefaction potential. *Journal of the Soil Mechanics and Foundations division*, 97(9), 1249-1273.

Seed H. B., and Idriss, I. M. (1982). Ground Motions and Soil Liquefaction During
Earthquakes, Earthquake Engineering Research Institute, Oakland, CA, 134.

Seed, H. B., Idriss, I. M., & Arango, I. (1983). Evaluation of liquefaction potential using field performance data. Journal of geotechnical engineering, 109(3), 458-482.

Seed, H. B., Tokimatsu, K., Harder, L. F., & Chung, R. M. (1985). Influence of SPT procedures in soil liquefaction resistance evaluations. Journal of geotechnical engineering, 111(12), 1425-1445.

Seed, H. B., & De Alba, P. (1986). Use of SPT and CPT tests for evaluating the liquefaction resistance of sands. In Use of in situ tests in geotechnical engineering (pp. 281-302). ASCE.

Shibata, T., & Teparaksa, W. (1988). Evaluation of liquefaction potentials of soils using cone penetration tests. Soils and Foundations, 28(2), 49-60.

Stark, T. D., & Olson, S. M. (1995). Liquefaction resistance using CPT and field case histories. *Journal of geotechnical engineering*, 121(12), 856-869.

Stokoe, K. H., Roesset, J. M., Bierschwale, J. G., & Aouad, M. (1988, August). Liquefaction potential of sands from shear wave velocity. In Proceedings, 9nd World Conference on Earthquake (Vol. 13, pp. 213-218).

Suzuki, Y., Tokimatsu, K., Koyamada, K., Taya, Y., & Kubota, Y. (1995). Field correlation of soil liquefaction based on CPT data. In Proceedings of *the International Symposium on Cone Penetration Testing* (Vol. 2, pp. 538-588).

Terzaghi K, Peck RB (1948) Soil mechanics in engineering practice. Wiley, New York

Tsuchida, H. and Hayashi, S. (1971): "Estimation of liquefaction potential of sandy soils," Third Joint Meeting of U.S. and Japan Panel on Wind and Seismic Effects, UJNR, Tokyo, pp.1-16.

Tokimatsu, K., & Uchida, A. (1990). Correlation between liquefaction resistance and shear wave velocity. Soils and foundations, 30(2), 33-42.

Tokimatsu, K., and Yoshimi, Y. (1983). "Empirical correlation of soil liquefaction based on SPT N-value and fines content." Soils and Foundations, 23(4), 56-74.

Toprak, S., Holzer, T. L., Bennett, M. J., & Tinsley III, J. C. (1999, August). CPT-and SPT-based probabilistic assessment of liquefaction. In Proc., 7th US–Japan Workshop on Earthquake Resistant Design of Lifeline Facilities and Countermeasures against Liquefaction (pp. 69-86). Buffalo, NY: Multidisciplinary Center for Earthquake Engineering Research.

Xue, X., & Liu, E. (2017). Seismic liquefaction potential assessed by neural networks. Environmental Earth Sciences, 76, 1-15.

Youd, T. L., & Idriss, I. M. (2001). Liquefaction Resistance of Soils: Summary Report from the 1. Geotechnical and Geoenvironmental Eng. In ASCE (Vol. 127, No. 10, pp. 817-33).

Zhang, W., & Goh, A. T. (2016). Evaluating seismic liquefaction potential using multivariate adaptive regression splines and logistic regression. *Geomech. Eng*, *10*(3), 269-284.

Zhang, Y. G., Qiu, J., Zhang, Y., & Wei, Y. (2021a). The adoption of ELM to the prediction of soil liquefaction based on CPT. *Natural Hazards*, *107*(1), 539-549.

Zhang, Y., Qiu, J., Zhang, Y., & Xie, Y. (2021b). The adoption of a support vector machine optimized by GWO to the prediction of soil liquefaction. Environmental Earth Sciences, 80, 1-9.

Zhou, J., Huang, S., Wang, M., & Qiu, Y. (2021). Performance evaluation of hybrid GA–SVM and GWO–SVM models to predict earthquake-induced liquefaction potential of soil: a multi-dataset investigation. *Engineering with Computers*, 1-19.

Zhou, J., Li, E., Wang, M., Chen, X., Shi, X., & Jiang, L. (2019). Feasibility of stochastic gradient boosting approach for evaluating seismic liquefaction potential based on SPT and CPT case histories. Journal of Performance of Constructed Facilities, 33(3), 04019024.